Modeling oscillatory microtubule polymerization

Martin Hammele and Walter Zimmermann
Theoretical Physics, University of Saarland, D-66041 Saarbrücken, Germany
(Received 1 October 2002; published 14 February 2003)

Polymerization of microtubules is ubiquitous in biological cells and under certain conditions it becomes oscillatory in time. Here, simple reaction models are analyzed that capture such oscillations as well as the length distribution of microtubules. We assume reaction conditions that are stationary over many oscillation periods, and it is a Hopf bifurcation that leads to a persistent oscillatory microtubule polymerization in these models. Analytical expressions are derived for the threshold of the bifurcation and the oscillation frequency in terms of reaction rates, and typical trends of their parameter dependence are presented. Both, a catastrophe rate that depends on the density of guanosine triphosphate liganded tubulin dimers and a delay reaction, such as the depolymerization of shrinking microtubules or the decay of oligomers, support oscillations. For a tubulin dimer concentration below the threshold, oscillatory microtubule polymerization occurs transiently on the route to a stationary state, as shown by numerical solutions of the model equations. Close to threshold, a so-called amplitude equation is derived and it is shown that the bifurcation to microtubule oscillations is supercritical.

DOI: 10.1103/PhysRevE.67.021903 PACS number(s): 87.10.+e, 47.54.+r, 87.16.Ka, 87.17.Aa

I. INTRODUCTION

Microtubules are cylindric filaments that are used in cells for many different purposes, being vitally involved in cell motility and division, organelle transport, and cell morphogenesis and organization [1]. The precise ways in which microtubules achieve their amazing variety of cellular functions is not fully understood yet. Microtubules in cells are generally dynamic, they assemble, disassemble or rearrange on a time scale of minutes. GTP (guanosine triphosphate) hydrolysis is apparently the driving force of microtubule physiology.

The rich nonequilibrium dynamics of microtubules, including nucleation, polymerization kinetics, etc. [2,3], is attracting considerable attention, both experimentally and theoretically [4–18]. Two phenomena in this area, the dynamical instability of microtubules [4] and the oscillatory polymerization [5–12], have already challenged theoretical modeling for a while [13–18].

Oscillations during microtubule polymerization have been observed either when GTP is regenerated enzymatically from endogenous GDP (guanosine diphosphate) [5,7,9,11] or when some amount of GTP is provided at the beginning or during an experiment. In the latter case, oscillations occur only as a transient, because GTP is either consumed or some reactions steps may be inhibited due to the accumulation of GDP [8]. If both possibilities are combined, the length of a transient regime depends on the initial concentrations of GTP and GDP and on the capacity to regenerate GTP. Present models for microtubule polymerization focus mainly on a description of transiently occurring oscillations, and the solutions of the respective models are mostly numerical [6,15,17].

In recent *in vitro* experiments, however, the capacity to regenerate GTP has been enhanced and extended up to several hours [19]. Compared to a typical oscillation period during microtubule polymerization, which is of the order of 1 min, the reaction conditions in these experiments are almost quasistationary over a long range of time. Therefore we focus on modeling microtubule polymerization for time-independent regeneration conditions. As a starting point we take common reduced models, where several elementary processes of the real biochemical reaction are described by a few effective reaction steps as explained in Sec. II, cf. Refs. [6,7,15,17]. Reductions of complex chemical reaction schemes are quite common, and a famous example is the so-called oregonator [20], which is a reduced model for the legendary Belousov-Zhabotinsky reaction [21]. However, since microtubules are long filaments, there are essential differences between the polymerization of microtubule filaments and common chemical reactions. For instance, microtubules may undergo an orientational ordering transition beyond a critical filament density [22], a phenomenon that does not occur in common chemical reactions. Accordingly, the length distribution of microtubules is explicitly taken into account for all variants of models investigated in this work. Such models are the basis of future work on interesting pattern-formation phenomena related to the interplay between orientational ordering of filaments and the kinetics involved in filament growth [23].

In addition, we focus on model variants that include the possibility of an oscillatory microtubule polymerization and that allow analytical approaches. However, the reaction steps, such as nucleation, growth, and decay of microtubules or the rate limiting factors of oligomer decay or tubulin regeneration, which have been identified to be crucial for oscillations [5–8,11], are taken into account. Moreover, we address the question whether microtubule oscillations occur transiently or in a persistent manner beyond a Hopf bifurcation. Whether such a Hopf bifurcation takes place supercritically or subcritically is investigated in terms of the so-called amplitude expansion.

It is not a major goal of this work to achieve quantitative agreement between the results obtained with phenomenological models and experimental measurements. However, since the present understanding of the mechanism leading to oscillatory microtubule polymerization is incomplete, reduced models may be an appropriate tool for working out

typical trends that may be testable in experiments. For comparison it is very helpful that, for reduced models, trends may be worked out analytically and may be presented by simple formulas. A number of spatiotemporal phenomena involving microtubule polymerization call for a better understanding too [10,24,25], but also in this case, simple and effective models are indispensable in order to keep the modeling tractable [26].

At the transition to oscillatory polymerization, the stationary state becomes sensitive against small perturbations, which grow or decay exponentially, $\propto e^{\sigma t}$. Here the exponential factor $\sigma=\sigma_r\pm i\omega_c$ is the sum of the so-called growth rate σ_r and the oscillation frequency $\omega_c\neq 0$. Below the bifurcation point, the growth rate $\sigma_r<0$ is negative and the perturbations are damped. Beyond the bifurcation point, σ_r is positive and the stationary polymerization state is unstable against oscillatory perturbations. Hence the Hopf bifurcation to oscillatory polymerization takes place when the real part σ_r of both roots passes zero. The investigation of the polymerization dynamics beyond the Hopf bifurcation requires in most cases a numerical analysis of the basic reaction equations. However, close to threshold, σ_r is small and the oscillation of the polymerization, described by the real part of $e^{i\omega_c t}$, is much faster than the temporal evolution of the complex valued amplitude $A(t)$ of the oscillations. Therefore the oscillation may be written as a product of both factors, i.e., $\propto A(t)e^{i\omega_c t}$, and there is a very general approach, the so-called amplitude expansion, for separating the dynamics at these two disparate time scales [27,28]. The amplitude equation describing the evolution of the amplitude $A(t)$ is obtained by a perturbation expansion of the reaction equations with respect to the slowly varying amplitude $A(t)$, and it is of the form

$$\tau_0\partial_t A=\varepsilon(1+ia)A-g(1+ic)|A|^2A. \tag{1}$$

The control parameter ε measures the relative distance from the bifurcation point and τ_0 is the relaxation time defined by $\tau_0=\varepsilon/\sigma_r$, which depends on the system. If the coefficient g of the nonlinear term is positive, the bifurcation to the oscillatory state is supercritical and if it is negative, the bifurcation is subcritical. The imaginary parts of the prefactors describe the linear and nonlinear frequency dispersion. Especially about the extension Eq. (1) including spatial degrees of freedom, there exists a rich literature as summarized, e.g., in a recent review [29]. Here, we calculate the coefficients of the universal equation (1) for microtubule polymerization and we discuss their variation in terms of reaction rates.

In Sec. II we describe the main steps of the reaction cycle for microtubule polymerization, and the respective equations for two models are presented. The time-independent solutions for the stationary polymerization are given for both models analytically in Sec. III. Those become unstable against oscillatory perturbations in the range of high tubulin-dimer density. The respective linear stability analysis and the derivation of the oscillation threshold are given in Sec. IV, including their dependence on the reaction parameters. Readers who are mainly interested in numerical results about the oscillation threshold may proceed directly to Sec. IV A 4. The partial differential equations for growing and shrinking microtubules are of first order in the length of the microtubules and first order in time. Their straightforward discretization and numerical solution has to be considered with care, therefore a stable numerical scheme, which becomes exact close to the threshold of the Hopf bifurcation, is described in Sec. V. The derivation of the universal equation (1) is outlined in Sec. VI, whereas the technical details are given in the Appendix. With a summary and an outlook about modeling microtubule polymerization, we conclude this work in Sec. VII.

II. MODELS FOR MICROTUBULE POLYMERIZATION

Microtubule assembly and disassembly proceeds in several steps [1–3,5,7,8]. Aggregation of GTP liganded tubulin dimers, the so-called tubulin-*t*, to microtubules is started by heating up tubulin solutions to a temperature of about 30–37 °C in the presence of GTP. Then microtubules spontaneously nucleate and polymerize to long rigid polymers made up of α-β tubulin dimers. An increasing number of long microtubules in a solvent causes an increasing turbidity, and the amount of polymerized tubulin-*t* may be monitored by measuring this turbidity [6] or by x-ray scattering [8]. The nucleation of microtubules is a rather complex process and it is still a matter of debate whether the nucleation rate depends in experiments only on the initial concentration of tubulin-*t*, c_t, or during the polymerization on the temporally varying c_t [3,30]. But once microtubules are formed, they grow and the available tubulin-*t* dimers will be used up. The growth velocity of microtubules, v_g, is rather sensitive to temperature variations, but rather independent of c_t [30,31]. Growing microtubules may change their states to rapidly depolymerizing ones by the so-called *catastrophe* rate f_{cat}. In previous works for the catastrophe rate, mostly an exponential dependence on the tubulin-*t* concentration was assumed, i.e., $f_{cat}\sim\exp(-c_t/c_f)$ with some constant c_f [6,15]. Once microtubules have changed from growth to shrinking, they shrink rather quickly with a large velocity $v_s\gg v_g$.

During the depolymerization of microtubules they are fragmented into oligomers or directly into GDP liganded tubulin dimers, the so-called tubulin-*d* dimers. The oligomers themselves are believed to fragment further into tubulin-*d* dimers and the decay rate depends on the free GTP and GDP. Oligomers are stabilized by GDP and destabilized by GTP [8,11]. If an excess of GTP is available, then tubulin-*d* in solution will exchange its unit of GDP for GTP and each tubulin-*t* dimer resulting from such an exchange step is identical to the initial tubulin-*t* dimer. Such a regeneration step completes the whole microtubule polymerization cycle. If a continuous source of GTP is provided, for instance, by a regeneration process, this cycling may be continued over a long time [19]. The variation of the reaction rates of the polymerization cycle with the concentration c_t may depend on the specific experiment.

There are rather detailed models available to describe this reaction cycle of microtubule polymerization, see, e.g., Ref. [15]. As a simplification of this complex biochemical reac-

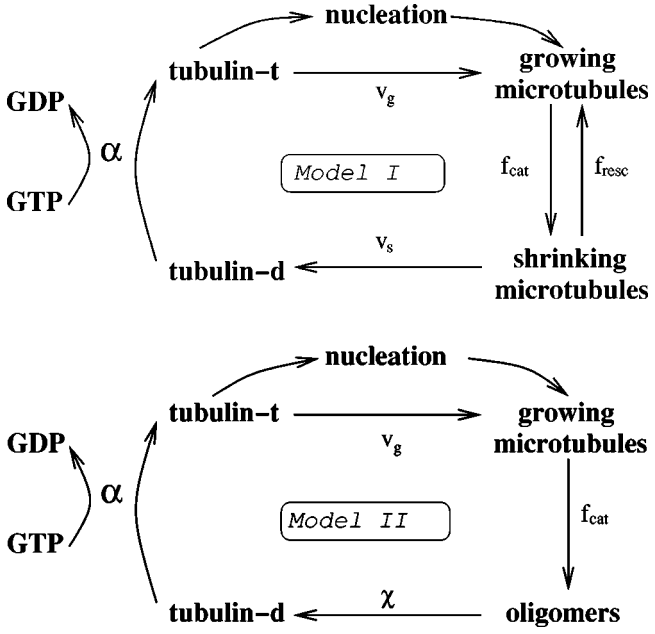

FIG. 1. Two models for the cycle of microtubule polymerization. Model I (upper cycle): Tubulin-*t* dimers may spontaneously form nuclei of microtubules that grow further by incorporating tubulin-*t* dimers. A growing microtubule may also change its state to a quickly depolymerizing one by the so-called *catastrophe* rate f_{cat}, but it may also change back to the polymerizing state by a so-called and rather small *rescue* rate f_{resc}. Tubulin-*d* dimers are released during this microtubule depolymerization, and the whole cycle becomes closed by regenerating them at a rate α back to tubulin-*t* dimers. Model II (lower cycle): Here the intermediate step of shrinking microtubules is replaced by oligomers, e.g., microtubules break off with a rate f_{cat} directly into oligomers and the oligomers themselves may break off with the rate χ into tubulin-*d* dimers. The rest of the cycle is identical to the upper cycle.

tion we only take into account as rate limiting factors one of the two intermediate steps of the polymerization cycle, either the dynamics of shrinking microtubules (upper cycle in Fig. 1) or the decay dynamics of oligomers (lower cycle in Fig. 1). Without both rate limiting factors there are no microtubule oscillations, but one is sufficient for oscillations. The two simplified reaction schemes, as sketched in Fig. 1, are analyzed in detail in this work.

A. Dynamics of growing microtubules

During microtubule polymerization there are many growing filaments in a unit volume and their length distribution may be described by a length- and time-dependent function $p_g(l,t)$, whose detailed form varies with the experimental conditions. A simple model for the dynamics of distribution of growing microtubules $p_g(l,t)$ is described by the following first-order differential equation [13,14]:

$$\partial_t p_g = -f_{cat} p_g - v_g \frac{\partial p_g}{\partial l}. \tag{2}$$

f_{cat} describes either the transition from the growing to the shrinking state of microtubules (model I) or the decay of growing microtubules into oligomers (model II). v_g is the growth velocity of the microtubules.

1. Growth velocity and catastrophe rate

In recent experiments with high tubulin-*t* concentration, the growth velocity v_g was rather independent of c_t [30]. Since we are mainly interested in the oscillatory behavior of microtubule polymerization, which occurs at high c_t concentrations, we assume a constant v_g in this work. In most of the present models, a c_t–dependent catastrophe rate f_{cat} is crucial for the oscillatory polymerization of microtubules. Rather common is an exponential c_t dependence [15]

$$f_{cat}(c_t) = f e^{-c_t/c_f}, \tag{3}$$

with the amplitude f and the decay constant c_f. However, also a linear c_t dependence

$$f_{cat}(c_t) = \overline{f}(c_u - c_t) \tag{4}$$

with an appropriate constant $c_u > c_t$ leads to an oscillatory microtubule polymerization, as we show in Sec. IV A. A hyperbolic c_t dependence of f_{cat}, as discussed in Ref. [16], also supports oscillating polymerization.

2. Nucleation and boundary conditions

The nucleation process of microtubules is rather complex and has been investigated in greater detail in Refs. [12,31,32] recently. The nucleation rate ν depends on the initial concentration c_0 of tubulin dimers, but it is rather independent of the temporal variation of c_t, as observed in recent experiments [30,3]. Accordingly, for a given initial concentration c_0 we assume a constant nucleation rate ν. The nucleation rate ν itself defines a boundary condition for the length distribution of growing microtubules, $p_g(l,t)$, at $l=0$,

$$p_g(l=0,t) = \frac{\nu}{v_g}. \tag{5}$$

B. Model I includes the dynamics of shrinking microtubules

In model I we take into account, as an intermediate step between growing microtubules and tubulin-*d* dimers, the dynamics of shrinking microtubules, $p_s(l,t)$. Here the catastrophe rate f_{cat} describes the transition of microtubules from the growing to the shrinking state. The depolymerization speed v_s of shrinking microtubules, $p_s(l,t)$, is mostly much larger than the growth velocity v_g. Having microtubules in two different states, one may also expect a transition from the shrinking back to the growing state, as described by a rate f_{resc}. So one has two coupled equations for the growing and shrinking microtubules [13,14]:

$$\partial_t p_g = -f_{cat} p_g + f_{resc} p_s - v_g \partial_l p_g, \tag{6a}$$

$$\partial_t p_s = f_{cat} p_g - f_{resc} p_s + v_s \partial_l p_s. \tag{6b}$$

The rescue rate f_{resc}, however, is usually very small in experiments and, therefore, it is neglected in this work. The boundary condition for shrinking microtubules is

$$p_s(l\to\infty,t)=0, \tag{7}$$

because the transition from growing to shrinking microtubules is the only source for the shrinking ones and $p_g(l\to\infty,t)$ vanishes for large values of l.

The temporal evolution of the concentration of the tubulin-t dimers, c_t, and tubulin-d dimers, c_d, is described by two equations as follows:

$$\partial_t c_t = -\gamma v_g \int_0^\infty dl\, p_g(l,t) + \alpha c_d, \tag{8a}$$

$$\partial_t c_d = \gamma v_s \int_0^\infty dl\, p_s(l,t) - \alpha c_d. \tag{8b}$$

The first term in Eq. (8a) describes the consumption of tubulin-t during the polymerization (growth) of microtubules and γ is a length factor describing the number of tubulin dimers that are incorporated in a unit length of microtubules. c_t is regenerated from c_d by exchanging the unit GDP for GTP, and this regeneration process, described by the rate α, occurs in Eq. (8a) as a source and in Eq. (8b) as a sink. Tubulin-d dimers are released during the depolymerization of microtubules $p_s(l,t)$ and this source is described by the integral in Eq. (8b).

Tubulin dimers may be a constituent of growing or shrinking microtubules, or they carry GTP or GDP as single dimers, but altogether they are conserved as expressed by the condition

$$c_t + c_d + \gamma L = c_0. \tag{9}$$

Here c_0 describes the overall concentration of tubulin dimers and $L(t)$ is the integrated length of all microtubules per unit volume,

$$L(t) = \int_0^\infty dl\, l[p_g(l,t) + p_s(l,t)]. \tag{10}$$

The tubulin-d concentration c_d may be eliminated from Eq. (8a) by using the conservation condition (9). On the other hand, Eq. (9) in combination with Eqs. (6) and (8a) yields an equation that is identical to Eq. (8b). Hence Eqs. (6a) and (6b) together with

$$\partial_t c_t = -\gamma \int_0^\infty dl\,[v_g p_g + \alpha l(p_g + p_s)] + \alpha(c_0 - c_t) \tag{11}$$

describe the polymerization dynamics of microtubules for model I, whereby a constant growth and shrinking velocity is assumed in this work.

1. Rescaling of model I

After rescaling time t and length l, i.e.,

$$t' = \alpha t, \quad l' = \frac{\alpha}{v_g} l, \tag{12}$$

it is easy to see that model I may be characterized by a set of dimensionless parameters

$$\gamma\frac{v_g}{\alpha}, \quad \frac{v_s}{v_g}, \quad \frac{\nu}{\alpha}, \quad \frac{c_0}{c_f}, \quad \frac{f_{resc}}{\alpha}. \tag{13}$$

Some of these dimensionless quantities may be further combined to other dimensionless parameters as, for instance, in the threshold condition given in Sec. IV A.

2. Reduced model

Since the depolymerization velocity v_s is much larger than the growth velocity v_g one may also consider the limit $v_s \gg v_g$. In this case the shrinking microtubules decompose nearly instantaneously into tubulin-d dimers, and growing microtubules decay effectively, due to the short life time of the shrinking microtubules, into tubulin-d dimers. In order to describe this direct decay, the source term in Eq. (8b), $\gamma v_s \int_0^\infty dl\, p_s(l,t)$, must be replaced by $\gamma f_{cat} \int_0^\infty dl\, l\, p_g(l,t)$. Eliminating again the density c_d, one ends up with a reduced model for only two densities:

$$\partial_t p_g = -f_{cat} p_g - v_g \partial_l p_g, \tag{14a}$$

$$\partial_t c_t = -\gamma \int_0^\infty dl\,(v_g + \alpha l) p_g + \alpha(c_0 - c_t). \tag{14b}$$

This simplified model reproduces essential aspects of the stationary polymerization of microtubules as described in Sec. III.

C. Model II includes the dynamics of oligomers

Oligomers occur as an intermediate product during the decay of microtubules and they are made of several tubulin dimers. This intermediate product is ignored in model I. Here in model II, after the so-called catastrophe, we ignore the dynamics of shrinking microtubules as an intermediate step and instead we take into account the (decay) dynamics of oligomers. Therefore, the catastrophe rate f_{cat} in Eq. (2) describes for model II a direct transition of growing microtubules into oligomers. Furthermore, it is assumed that oligomers decay with the rate χ into tubulin-d dimers. The concentration of oligomers is denoted by c_{oli}, and its dynamics as well as that of c_d are described by the two equations

$$\partial_t c_{oli} = \eta f_{cat} \int_0^\infty dl\, l\, p_g(l,t) - \chi c_{oli}, \tag{15a}$$

$$\partial_t c_d = \chi\lambda c_{oli} - \alpha c_d. \tag{15b}$$

η is a measure for the number of oligomers per unit length of the microtubules and λ is a measure for the number of tubulin dimers per oligomer. Oligomers decaying with the rate χ build a source term in the equation for tubulin-*d* dimers in Eq. (15b).

The conservation law for the concentration of all tubulin dimers takes the form

$$c_t + c_d + \lambda c_{oli} + \eta\lambda \int_0^\infty dl\, l p_g(l,t) = c_0 . \tag{16}$$

The equation for the growing microtubules is the same as for model I, cf. Eq. (2), but in the equation for c_t, cf. Eq. (8a), one has to replace the length factor γ by the product $\eta\lambda$. Eliminating c_{oli}, model II is described by Eqs. (2) and (8a) together with the following dynamical equation for c_d:

$$\partial_t c_d = \chi\left(c_0 - c_t - c_d - \eta\lambda \int_0^\infty dl\, l p_g \right) - \alpha c_d . \tag{17}$$

As a boundary condition for the growing microtubules, we again use Eq. (5) with a constant nucleation rate ν. For model II we only consider the catastrophe rate given in Eq. (3). This again guarantees a nonlinear feedback of the dynamics of the tubulin-*t* dimers to the dynamics of the growing microtubules.

Reduced model

Similar to model I, model II also becomes identical to the model described by Eqs. (14) in the limit $\chi \to \infty$. If we assume a very fast dissociation of oligomers into tubulin-*d* dimers, $\chi \gg 1$, we can neglect the intermediate state c_{oli}. In this case the source term in Eq. (15b), $\chi\lambda c_{oli}$, can be replaced by the source in Eq. (15a), cf. $\eta\lambda f_{cat}\int_0^\infty dl\, l\, p_g$, which describes the direct decay of growing microtubules into tubulin-*d* dimers. After replacing c_d and setting $\gamma = \eta\lambda$ in Eq. (8a), we again obtain with the help of the conservation law (16) the simple reduced model as described by Eqs. (14).

III. STATIONARY SOLUTIONS

A polymerization cycle with a stationary length distribution of microtubules and time-independent dimer concentrations c_t, c_d or oligomer concentration c_{oli} are one type of solutions of the model equations described in Sec. II. For this stationary state, the various polymerization steps, such as nucleation, assembly and disassembly of microtubules, as well as the regeneration of tubulin-*d* dimers are in a balanced state. Under certain conditions a stationary polymerization is observed in experiments [31]. However, it may become unstable against oscillatory perturbations if the initial tubulin dimer concentration c_0 is large enough, as shown in Sec. IV.

A. Model I

Equations (6) are first-order linear differential equations with respect to the length *l*, and in the stationary case these

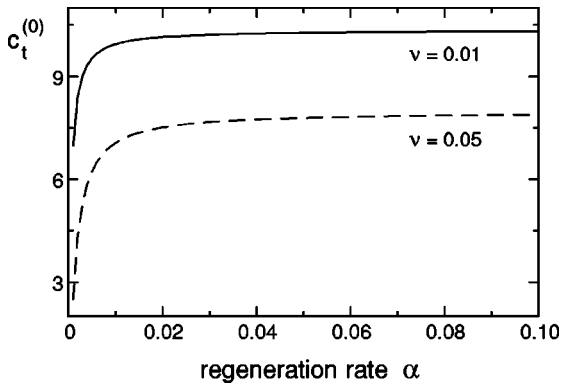

FIG. 2. The tubulin-*t* concentration $c_t^{(0)}$ for the stationary polymerization state of model I is shown as a function of the regeneration rate α and for two different values of the nucleation rate ν. The velocity ratio between the growing and shrinking microtubules is $\beta = v_g/v_s = 0.1$ and the rest of the parameters are $c_0 = 120$, $v_g = 0.1$, $c_f = 3$, $f = 0.1$, $\gamma = 1$.

equations have exponentially decaying solutions, which take in the limit of a vanishing rescue rate the form

$$p_{g,s}^{(0)}(l) = \frac{\nu}{v_{g,s}} \exp\left(-\frac{f_{cat}^{(0)}}{v_g} l \right). \tag{18}$$

The catastrophe rate $f_{cat}^{(0)}$ may be given either by Eq. (3) or Eq. (4) but in both cases the stationary tubulin-*t* concentration, denoted by $c_t^{(0)}$, is determined self-consistently as described below. The stationary solutions $p_{g,s}^{(0)}$ allow an analytical calculation of the integrals in Eq. (11), and a nonlinear equation in $c_t^{(0)}$ follows:

$$c_0 - c_t^{(0)} = \frac{\nu\gamma v_g}{f_{cat}^{(0)}} \left(\frac{1}{\alpha} + \frac{1}{f_{cat}^{(0)}} (1+\beta) \right). \tag{19}$$

From this equation the stationary tubulin concentration $c_t^{(0)}$ can be determined as a function of the overall concentration of tubulin dimers c_0 and as a function of the other parameters. In Eq. (19) the abbreviation for the velocity ratio

$$\beta = \frac{v_g}{v_s} \tag{20}$$

has been introduced, and the respective length distributions $p_g^{(0)}$ and $p_s^{(0)}$ follow for a given value of $c_t^{(0)}$ via Eqs. (18). The stationary value $c_t^{(0)}$ for the reduced model, described by Eqs. (14), follows from Eq. (19) in the limit $\beta \to 0$.

In the range of α much larger than the catastrophe rate $f_{cat}^{(0)}$, the stationary tubulin-*t* concentration $c_t^{(0)}$ becomes independent of it, because all tubulin-*d* dimers that are released during the depolymerization, are immediately regenerated to tubulin-*t* dimers. Both a large nucleation rate ν and a large growth velocity v_g lead to a high consumption of tubulin-*t* and, therefore, to a lower stationary concentration $c_t^{(0)}$. This tendency is illustrated by the difference between the two curves in Fig. 2. On the other hand, large values of the amplitude of the respective catastrophe rate, either f or $\overline{f}$,

act against long microtubules, which consist of many tubulin dimers and, therefore, enhance the densities $c_t^{(0)}$ and $c_d^{(0)}$. The length distribution of the growing respective shrinking microtubules is determined by $v_g/f_{cat}^{(0)}$, which also depends via the catastrophe rate on the concentration $c_t^{(0)}$.

These tendencies become even more obvious if the linear dependence of the catastrophe rate in Eq. (4) is chosen for the special case $c_u=c_0$ and Eq. (19) is expanded in the limit of small and large values of α. In both cases, we obtain the simple formulas

$$c_t^{(0)}=c_0-\left(\frac{\nu\gamma v_g(1+\beta)}{\overline{f}}\right)^{1/3} \quad (\alpha\gg\overline{f}), \tag{21a}$$

$$c_t^{(0)}=c_0-\left(\frac{\nu\gamma v_g}{\alpha\overline{f}}\right)^{1/2} \quad (\alpha\ll\overline{f}), \tag{21b}$$

which reflect the described tendencies.

B. Model II

Stationary solutions for model II can be calculated in a similar manner as discussed in the preceding section for model I. The length distribution of growing microtubules is again given by Eq. (18) and the integral in Eq. (17) can be calculated analytically. c_d may be eliminated from Eq. (17) by using Eq. (8a) with $\dot{c}_t=0$ and by setting $\gamma=\eta\lambda$. Then the nonlinear equation for tubulin-t dimers $c_t^{(0)}$ takes the form

$$c_0-c_t^{(0)}=\frac{\nu\eta\lambda v_g}{f_{cat}^{(0)}}\left(\frac{1}{\alpha}+\frac{1}{\chi}+\frac{1}{f_{cat}^{(0)}}\right). \tag{22}$$

Equation (22) is invariant under the permutation $\alpha\leftrightarrow\chi$. If α and χ become much larger than the catastrophe rate, the stationary concentration $c_t^{(0)}$ becomes rather independent of both. In the limits $v_s\to\infty$ in Eq. (19) and $\chi\to\infty$ in Eq. (22), we again obtain the concentration $c_t^{(0)}$ for the reduced model. No stationary solution is possible in the limit $\chi\to 0$, because in this limit all tubulin-d dimers are stored in oligomers and the polymerization cycle becomes interrupted.

IV. THRESHOLD FOR OSCILLATORY POLYMERIZATION

Stationary microtubule polymerization becomes unstable against oscillating modes in the range of high tubulin dimer concentrations c_0, and the parameter range where this happens is calculated by a linear stability analysis. Starting from the model equations given in Sec. II, we derive linear equations for small perturbations with respect to the stationary state, and such perturbations exhibit an exponential time dependence $e^{\sigma t}$. For the exponential factor σ, we derive a nonlinear equation from which both the critical dimer concentration c_{0c} and the critical frequency ω_c for the Hopf bifurcation are calculated numerically for various parameter combinations and in limiting cases also analytically.

A. Model I

We introduce small perturbations $p_{g,s}^{(1)}$ and $c_t^{(1)}$ with respect to the stationary solutions $p_{g,s}^{(0)}$ and $c_t^{(0)}$ as determined in the preceding section. With the ansatz

$$p_{g,s}=p_{g,s}^{(0)}+p_{g,s}^{(1)}, \tag{23a}$$

$$c_t=c_t^{(0)}+c_t^{(1)}, \tag{23b}$$

one obtains, after linearization of Eqs. (6) and (11), the following set of linear equations describing the dynamics of the perturbations:

$$\partial_t p_g^{(1)}=-(f_{cat}^{(0)}+v_g\partial_l)p_g^{(1)}-p_g^{(0)}f_{cat}^{(1)}, \tag{24a}$$

$$\partial_t p_s^{(1)}=v_s\partial_l p_s^{(1)}+f_{cat}^{(0)}p_g^{(1)}+p_g^{(0)}f_{cat}^{(1)}, \tag{24b}$$

$$\partial_t c_t^{(1)}=-\alpha c_t^{(1)}-\gamma\int_0^\infty dl[v_g p_g^{(1)}+\alpha l(p_g^{(1)}+p_s^{(1)})]. \tag{24c}$$

Here, $f_{cat}^{(1)}$ is the first-order contribution of an expansion of the catastrophe rate $f_{cat}=f_{cat}^{(0)}+f_{cat}^{(1)}+\cdots$ with respect to the perturbation $c_t^{(1)}$:

$$f_{cat}^{(1)}=-f_{cat}^{(0)}\frac{c_t^{(1)}}{c_f}. \tag{25}$$

Since the first-order linear equations (24) have constant coefficients, their solutions depend exponentially on time and $c_t^{(1)}$ may be written as

$$c_t^{(1)}=Ae^{\sigma t}+\text{c.c.} \tag{26}$$

(c.c. denotes the complex conjugate). With this ansatz the three equations in Eq. (24) can easily be integrated and the solutions for the growing and shrinking microtubules are given by

$$p_g^{(1)}=-\frac{\nu f_{cat}^{(0)}}{v_g c_f\sigma}\exp\left(\sigma t-\frac{f_{cat}^{(0)}}{v_g}l\right)\left[\exp\left(-\frac{\sigma}{v_g}l\right)-1\right]A+\text{c.c.}, \tag{27a}$$

$$p_s^{(1)}=-\frac{\nu f_{cat}^{(0)}}{v_s c_f\sigma}\exp\left(\sigma t-\frac{f_{cat}^{(0)}}{v_g}l\right)\left[k_1\exp\left(-\frac{\sigma}{v_g}l\right)+k_2+K\exp\left(\frac{\sigma}{v_s}l\right)\right]A+\text{c.c.} \tag{27b}$$

Herein, we have introduced the abbreviations

$$k_1=\frac{f_{cat}^{(0)}}{\sigma(1+\beta)+f_{cat}^{(0)}},$$

$$k_2=\frac{\sigma-f_{cat}^{(0)}}{f_{cat}^{(0)}+\sigma\beta}, \tag{28}$$

and the boundary condition in Eq. (7) requires a vanishing integration constant $K=0$. The boundary condition for the time-dependent part of the growing microtubules, $p_g^{(1)}(l=0,t)=0$, is also fulfilled. According to the analytic expressions for $p_g^{(1)}$ and $p_s^{(1)}$ given in Eqs. (27) both may be eliminated in Eq. (24c). The remaining integral in Eq. (24c) can be calculated analytically and the nonlinear dispersion relation for σ follows:

$$1+\sigma(\sigma+\alpha)G+\frac{\alpha}{f_{cat}^{(0)}}\left(1+\beta\frac{f_{cat}^{(0)}-\sigma}{f_{cat}^{(0)}+\sigma\beta}\right)-\frac{f_{cat}^{(0)}}{f_{cat}^{(0)}+\sigma}\times\left[1+\frac{\alpha}{f_{cat}^{(0)}+\sigma}\left(1+\beta\frac{f_{cat}^{(0)}}{f_{cat}^{(0)}+\sigma(1+\beta)}\right)\right]=0, \tag{29}$$

with a reduced parameter

$$G=\frac{c_f}{\gamma\nu v_g} \tag{30}$$

for the catastrophe rate given in Eq. (3) and with

$$G=\frac{f_{cat}^{(0)}}{f\gamma\nu v_g} \tag{31}$$

for the rate given in Eq. (4). After a few rearrangements, the dispersion relation in Eq. (29) can be written as a fourth-order polynomial in σ,

$$\sigma^4 G\beta(1+\beta)+\sigma^3 G[\alpha\beta(1+\beta)+f_{cat}^{(0)}(1+3\beta+\beta^2)]+\sigma^2[G\alpha f_{cat}^{(0)}(1+3\beta+\beta^2)+(\beta+2Gf_{cat}^{(0)2})(1+\beta)]+\sigma[\alpha(1+\beta)(1+\beta+2Gf_{cat}^{(0)^2})+Gf_{cat}^{(0)^3}+f_{cat}^{(0)}\times(1+2\beta)]+\alpha f_{cat}^{(0)}[2+2\beta+Gf_{cat}^{(0)^2}]+f_{cat}^{(0)^2}=0. \tag{32}$$

This polynomial describes the linear stability of the stationary solutions given by Eqs. (18) and (19) completely and they are unstable in the parameter range where the *growth rate* becomes positive, $\mathrm{Re}(\sigma)>0$. Keeping, for instance, all parameters besides the dimer concentration c_0 fixed, the *neutral stability condition* $\mathrm{Re}(\sigma)=0$ provides an equation for the critical dimer concentration c_{0c}. For concentrations larger than this critical value, $c_0>c_{0c}$, the stationary solutions are unstable.

The smallest critical dimer concentrations c_{0c} for an oscillatory polymerization are required if the parameters α, β, and G take intermediate values, as discussed in greater detail below. At the threshold, the real part $\mathrm{Re}(\sigma)=0$ vanishes and the imaginary part of σ is the so-called Hopf frequency $\omega_c=\mathrm{Im}(\sigma)$. In this special case with a purely imaginary σ, the polynomial in Eq. (32) can be decomposed into its real and imaginary parts, giving two coupled equations for the determination of the two unknowns $f_{cat}^{(0)}$ and ω_c. Having determined $f_{cat}^{(0)}$ numerically, c_{0c} may be calculated via Eq. (19).

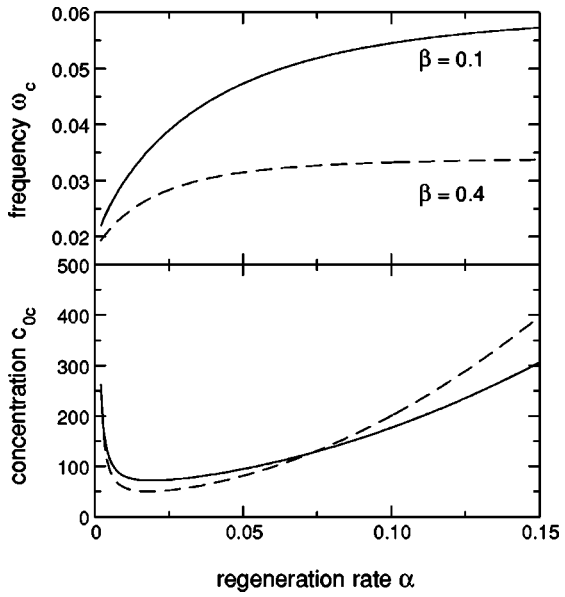

FIG. 3. The critical tubulin dimer concentration c_{0c} and the critical oscillation frequency ω_c are given at the threshold of the Hopf bifurcation as functions of the regeneration rate α, for two values of $\beta=v_g/v_s$ and for the constant $G=3000$. The catastrophe rate given in Eq. (3) has been used with the parameter values $f=0.1$ and $c_f=3$.

1. Limiting cases for the rate in Eq. (3)

For the limiting cases $\beta\to 0$, $\beta\to\infty$, $\alpha\to 0$, and $\alpha\to\infty$, analytical expressions can be given for both the threshold concentration c_{0c} and the Hopf frequency ω_c. This is explained first for the catastrophe rate given by Eq. (3) and for the parameter G given in Eq. (30). At threshold, one has $\sigma=i\omega_c$ and two equations follow from the nonlinear dispersion relation in Eq. (32) which determine the two unknowns ω_c and $f_{cat}^{(0)}$. The critical initial concentration c_{0c} follows via $f_{cat}^{(0)}$ from Eq. (19).

(a) $\alpha\to\infty$. In this limit one obtains from Eq. (32)

$$f_{cat}^{(0)}=\frac{1}{\alpha G}\frac{1+\beta}{1+\beta+\beta^2}, \tag{33a}$$

$$\omega_c=\sqrt{\frac{1+\beta}{G\beta}}. \tag{33b}$$

Accordingly the critical tubulin concentration diverges as $c_{0c}\propto\alpha^2$, which agrees with the full numerical results shown in Fig. 3, besides small logarithmic corrections. In this limit, the Hopf frequency ω_c becomes independent of α and with increasing values of β it decreases slightly to a constant value $\omega_c\sim\sqrt{1/G}$.

(b) $\alpha\to 0$. In this case $\omega_c\sim\sqrt{1/G}$ also becomes independent of α and the catastrophe rate vanishes as $f_{cat}^{(0)}\sim\alpha$. Therefore the critical tubulin concentration diverges according to Eq. (19) as $c_{0c}\sim\alpha^{-2}$.

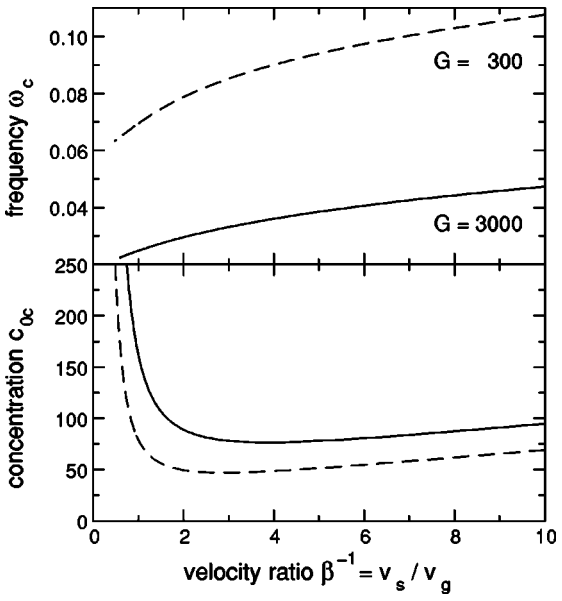

FIG. 4. The critical tubulin concentration c_{0c} and the frequency ω_c are given at the Hopf bifurcation as functions of the ratio between the shrinking and growth velocity of microtubules, $v_s/v_g = \beta^{-1}$, for $\alpha = 0.05$ and for two different values of G. The c_t dependence of the catastrophe rate as given in Eq. (3) has been used with the same parameters as in Fig. 3.

(c) $\beta \to 0$. In this limit, one obtains

$$f_{cat}^{(0)} = \sqrt{\frac{\beta}{G}} \quad \text{and} \quad \omega_c = \left(\frac{\alpha^2}{G}\right)^{1/4}\left(\frac{1}{\beta}\right)^{1/4}. \tag{34}$$

The Hopf frequency diverges with increasing values of the shrinking velocity as $\omega_c \sim v_s^{1/4}$, in agreement with the numerical results shown in Fig. 4. With this expression for $f_{cat}^{(0)}$, one obtains, via Eq. (19) for the critical initial concentration, $c_{0c} \sim G/\beta + c_f \ln[f(G/\beta)^{1/2}]$. For medium parameter values, this is essentially $c_{0c} \propto 1/\beta$ as indicated in Fig. 4.

In experiments, the shrinking velocity was always larger than the growth velocity, therefore the limit $\beta \to \infty$ is discarded.

2. Limiting cases for the rate in Eq. (4)

The tendencies for the parameter dependence of the threshold for the Hopf bifurcation as discussed in Sec. IV A 1 are by far not a special property of the choice of the catastrophe rate in Eq. (3). Therefore we consider the same limiting cases as before for the catastrophe rate given in Eq. (4) and with G as defined in Eq. (31).

(a) $\alpha \to \infty$. In this limit one obtains from Eq. (32)

$$f_{cat}^{(0)} = \left(\frac{g(1+\beta)}{\alpha(1+\beta+\beta^2)}\right)^{1/2}, \tag{35a}$$

$$\omega_c = \frac{[\alpha g(1+\beta+\beta^2)(1+\beta)]^{1/4}}{\beta^{1/2}}, \tag{35b}$$

with $g = \bar{f}\gamma\nu v_g$. Hence the critical tubulin concentration required for a Hopf bifurcation diverges as $c_{0c} \propto \alpha$.

(b) $\alpha \to 0$. In this limit one has $f_{cat}^{(0)} \propto \alpha$, and $c_{0c} \propto \alpha^{-2}$ diverges too.

(c) $\beta \to 0$. For this limit, we obtain

$$f_{cat}^{(0)} = (g\beta)^{1/3}, \tag{36a}$$

$$\omega_c = g^{1/6}\alpha^{1/2}\left(\frac{1}{\beta}\right)^{1/3}. \tag{36b}$$

This confirms the importance of a finite ratio of $\beta = v_g/v_s$, because the threshold diverges for $\beta \to 0$, similar to the catastrophe rate given in Eq. (3).

3. Traveling waves solutions

At the threshold of the Hopf bifurcation, the rate σ is purely imaginary, $\sigma = i\omega_c$, and the expressions given in Eqs. (26) and (27) are oscillatory in time,

$$c_t^{(1)} = 2A\cos(\omega_c t), \tag{37a}$$

$$p_g^{(1)} = \frac{S_1}{v_g}\exp\left(-\frac{f_{cat}^{(0)}}{v_g}l\right)[\sin(\omega_c t) - \sin\{\omega_c(t - l/v_g)\}], \tag{37b}$$

$$p_s^{(1)} = -\frac{S_1}{v_s}\exp\left(-\frac{f_{cat}^{(0)}}{v_g}l\right)[k_2\sin(\omega_c t + \varphi_2) + k_1\sin\{\omega_c(t - l/v_g) + \varphi_1\}], \tag{37c}$$

whereby the following abbreviations for the amplitudes,

$$S_1 = \frac{2A\nu f_{cat}^{(0)}}{\omega_c c_f}, \tag{38a}$$

$$k_1 = \frac{\sqrt{f_{cat}^{(0)4} + \omega_c^2 f_{cat}^{(0)2}(1+\beta)^2}}{f_{cat}^{(0)2} + \omega_c^2(1+\beta)^2}, \tag{38b}$$

$$k_2 = \frac{\sqrt{(\omega_c^2\beta - f_{cat}^{(0)2})^2 + f_{cat}^{(0)2}\omega_c^2(1+\beta)^2}}{f_{cat}^{(0)2} + (\omega_c\beta)^2}, \tag{38c}$$

and phases,

$$\varphi_1 = -\arctan\left(\frac{\omega_c(1+\beta)}{f_{cat}^{(0)}}\right), \tag{39a}$$

$$\varphi_2 = \arctan\left(\frac{\omega_c f_{cat}^{(0)}(1+\beta)}{\beta\omega_c^2 - f_{cat}^{(0)2}}\right), \tag{39b}$$

have been introduced. The analytical expressions for $p_g^{(1)}$ and $p_s^{(1)}$ indicate that the time-dependent contribution to the length distribution of the microtubules includes homogeneous amplitude oscillations and waves with a wavelength ω_c/v_g that travel to larger values of the length l. Hence, the length distributions $p_{g,s}^{(1)}$ depend on two different length

scales, the decay length $v_g/f_{cat}^{(0)}$ and the wavelength v_g/ω_c of the traveling waves. With the explicit solutions for $c_t^{(1)}$ and $p_g^{(1)}$, the phase of the oscillating part of the tubulin-*d* concentration relative to the phase of $c_t^{(1)}$ as well as its oscillation amplitude is calculated via Eq. (8a).

4. Numerical results for the threshold of model I

Since σ is purely imaginary at the threshold of a Hopf bifurcation, $\sigma = i\omega_c$, the dispersion relation in Eq. (32) can be decomposed into its real and imaginary parts, and from these two equations the critical concentration c_{0c} and the frequency ω_c may be calculated numerically as a function of the parameters. The numerical calculations in this section are restricted to the exponential tubulin dependence of the catastrophe rate as given by Eq. (3).

The critical tubulin dimer concentration c_{0c} and the critical frequency ω_c at the Hopf bifurcation are shown in Fig. 3 as functions of the regeneration rate α and in Fig. 4 as functions of the velocity ratio $1/\beta = v_s/v_g$, whereby the reduced parameter G has been chosen at the values $G=3000$ and $G=300$, respectively. Since G includes a number of parameters, the curves in both figures represent a larger parameter set. In the limit of a vanishing regeneration and in the limit of very large values of α, where the regeneration process is much faster than any other process, the critical tubulin concentration c_{0c} diverges and, therefore, the Hopf bifurcation is suppressed. In addition, both figures indicate that the smallest values of the critical tubulin concentration c_{0c} are obtained at intermediate values of the parameters α, β, and G. The location of the threshold minima, however, depends on the actual values of the rest of the parameters. The frequency ω_c becomes rather small in the limit $\alpha \to 0$, and for large values of α, this frequency becomes independent of it, cf. Sec. IV A 1.

In Fig. 4 the threshold minimum is less pronounced than in Fig. 3, and in the limit $\beta = v_g/v_s \to 0$, the threshold c_{0c} increases linearly with v_s and in agreement with limits given in Sec. IV A 1. Accordingly, there is no Hopf bifurcation for the reduced model that follows in the limit $\beta \to 0$ as described in Sec. II B 2. Hence, the dynamics of shrinking microtubules is one essential degree of freedom favoring oscillating microtubule polymerization. The dynamics of oligomers, as discussed in Sec. IV B, is an alternative degree of freedom that favors oscillations.

For large values of v_s the frequency ω_c becomes large too, and the oscillation period becomes much shorter than any relaxational dynamics of p_g and c_t. According to the quick shrinking, the lifetime of a depolymerizing microtubule vanishes and, therefore, the amplitude of the density of shrinking microtubules is small too, $p_s \propto 1/v_s$. In other words, in the limit of large values of v_s, the intermediate step of shrinking microtubules may be neglected, and the transition from p_g to tubulin-*d* dimers is effectively a direct process as explicitly assumed for the reduced model. If either the regeneration or the shrinking dynamics becomes too fast, the Hopf bifurcation is suppressed. The two intermediate steps, the depolymerization and the regeneration, act obviously as antagonistic steps or jam processes that favor oscillations.

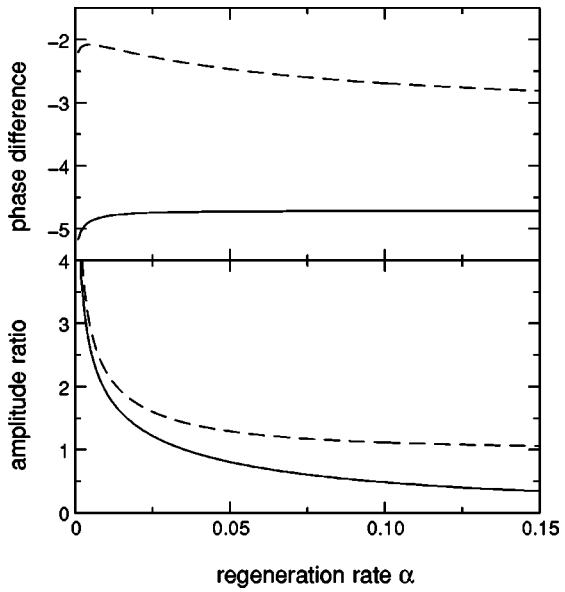

FIG. 5. In the upper part, the differences between the phases of the oscillating contributions of the tubulin-*d* concentration c_d (solid) and of the tubulin-*t* c_t as well as between $L(t)$ and c_t (dashed) are shown as functions of the regeneration rate α. In the lower part the ratios between the amplitudes of the oscillating contributions $c_d^{(1)}$ and $c_t^{(1)}$ (solid) as well as between the amplitudes of $L^{(1)}$ and $c_t^{(1)}$ (dashed) are shown. The rest of parameters are as in Fig. 3.

Since one has at threshold $\sigma = i\omega_c$, $p_g^{(1)}$ and $p_s^{(1)}$ in Eqs. (37b) and (37c) include both traveling wave contributions proportional to $\exp[-i(\omega_c t - kl)]$ with a wave number $k = \omega_c/v_g$ that always travel towards larger lengths of the microtubules. The length distribution is exponentially decaying on the length scale $v_g/f_{cat}^{(0)}$. If this is large compared to the wavelength $\lambda = 2\pi v_g/\omega_c$, as, for instance, in the limit $v_s \gg v_g$, then one has a kind of self-averaging in the respective integrals and the Hopf bifurcation is suppressed.

The phase difference between the oscillations of tubulin-*t* and the oscillations of the total amount of polymerized tubulin, described by $L(t)$ in Eq. (10), is another experimentally accessible quantity [33]. The difference between the phases of the oscillatory contributions of c_d and c_t as well as the difference between the phases of $L(t)$ and c_t are given in Fig. 5. These phase differences as well as the ratios between the amplitudes of the fields, cf. lower part of Fig. 5, are calculated at the threshold of the Hopf bifurcation by using the analytical solutions calculated in Sec. IV A 3.

For large values of α, tubulin-*d* is quickly regenerated into tubulin-*t* and, therefore, the density c_d becomes smaller as shown by the lower part in Fig. 5. In the opposite limit of small values of α, tubulin-*t* is consumed by nucleation and growth of microtubules, but the source, which is supplied by the regeneration of tubulin-*d*, decays and, therefore, one obtains large values for the ratio between the amplitudes of $c_d^{(1)}$ and $c_t^{(1)}$ as well as between the amplitudes of $L^{(1)}$ and $c_t^{(1)}$.

The decay of the ratio between the amplitudes of $L^{(1)}$ and $c_t^{(1)}$ is less obvious. $L^{(1)}=L_g^{(1)}+L_s^{(1)}$ has the two contributions $L_g^{(1)}=\gamma\int_0^\infty dl\, l\, p_g^{(1)}=\overline{A}\cos(\omega_c t+\varphi_{\overline{A}})$ and $L_s^{(1)}=\gamma\int_0^\infty dl\, l\, p_s^{(1)}=\overline{B}\cos(\omega_c t+\varphi_{\overline{B}})$. The two amplitudes $\overline{A}$ and $\overline{B}$ increase with the regeneration rate α. However, with increasing values of α, the phase difference $\varphi_{\overline{A}}-\varphi_{\overline{B}}$ increases as well up to unity, leading to an effective decay of the sum $L^{(1)}$ as shown by the lower part of Fig. 5.

The phase shifts of c_d and $L(t)$ with respect to the phase of c_t are rather independent of the regeneration rate α as shown in Fig. 5. The absolute values of these shifts are in qualitative agreement with the expectation as described in the following. At the maximum of c_t the catastrophe rate takes its minimum and, therefore, since the nucleation and the growth velocity are constant, $L(t)$ increases for a while, up to the moment when enough c_t is consumed, and the catastrophe rate increases again. Due to an increasing decay of microtubules, the maximum of the latter will also lead to a delayed maximum for c_d. For large values of α, the amount of polymerized tubulin is nearly in antiphase with respect to c_t, which is also mentioned in Ref. [15]. The slightly stronger α dependence of the phase difference between $L(t)$ and c_t is mainly due to the α dependence of shrinking microtubules p_s, because the relative phase of $p_g^{(1)}$ is nearly independent of α (see also Sec. IV B).

B. Model II

Here the stability of the stationary polymerization state of model II, described by $c_t^{(0)}$, $c_d^{(0)}$, and $p_g^{(0)}$, is investigated with respect to small perturbations $c_t^{(1)}$, $c_d^{(1)}$, and $p_g^{(1)}$. With the ansatz

$$p_g=p_g^{(0)}+p_g^{(1)}, \tag{40a}$$

$$c_{t,d}=c_{t,d}^{(0)}+c_{t,d}^{(1)}, \tag{40b}$$

the equations for model II are linearized with respect to these perturbations and one obtains the following set of linear differential equations with constant coefficients:

$$\partial_t p_g^{(1)}=-f_{cat}^{(1)}p_g^{(0)}-(f_{cat}^{(0)}+v_g\partial_l)p_g^{(1)}, \tag{41a}$$

$$\partial_t c_t^{(1)}=-\eta\lambda v_g\int_0^\infty dl p_g^{(1)}+\alpha c_d^{(1)}, \tag{41b}$$

$$\partial_t c_d^{(1)}=-\chi\left(c_t^{(1)}+c_d^{(1)}+\eta\lambda\int_0^\infty dl\, l\, p_g^{(1)}\right)-\alpha c_d^{(1)}. \tag{41c}$$

$f_{cat}^{(1)}$ is the first-order correction with respect to its value in the stationary state and it is given by Eq. (25).

The time-dependent contributions to the tubulin-t and tubulin-d dimer densities are described by

$$c_t^{(1)}=Ae^{\sigma t}+\text{c.c.}, \tag{42a}$$

$$c_d^{(1)}=EAe^{\sigma t}+\text{c.c.}, \tag{42b}$$

with the common complex amplitude A and relative complex factor E that describes via $E=|E|e^{i\varphi_d}$ the amplitude ratio $|E|$ as well as the phase difference φ_d between both fields. With the solution for growing microtubules as given in Eq. (27a) we can eliminate $c_t^{(1)}$, and $p_g^{(1)}$ in Eq. (41b) and we again obtain from the resulting solubility condition a nonlinear dispersion relation for the exponential factor σ,

$$\left(G\sigma+\frac{1}{\sigma+f_{cat}^{(0)}}\right)(\sigma+\alpha+\chi)+\alpha\chi\left(G+\frac{\sigma+2f_{cat}^{(0)}}{f_{cat}^{(0)}(\sigma+f_{cat}^{(0)})^2}\right)=0, \tag{43}$$

with $G=c_f/(\eta\lambda v_g\nu)$. After a few rearrangements of this equation, one obtains a fourth-order polynomial in σ for model II as well,

$$\begin{aligned}\sigma^4 f_{cat}^{(0)}G+\sigma^3 f_{cat}^{(0)}G(2f_{cat}^{(0)}+\alpha+\chi)+\sigma^2 f_{cat}^{(0)}[1+\alpha\chi G\\ +Gf_{cat}^{(0)}(2\chi+f_{cat}^{(0)}+2\alpha)]+\sigma[f_{cat}^{(0)}(f_{cat}^{(0)}+\alpha+\chi)+\alpha\chi\\ +f_{cat}^{(0)2}G\{2\alpha\chi+f_{cat}^{(0)}(\alpha+\chi)\}]+f_{cat}^{(0)}\alpha\chi(Gf_{cat}^{(0)2}+2)\\ +f_{cat}^{(0)2}(\alpha+\chi)=0,\end{aligned} \tag{44}$$

which determines the linear stability of the stationary polymerization for model II. Again we are interested in the neutrally stable case, $\mathrm{Re}(\sigma)=0$, which separates the stable from the unstable regime. At the neutral stability point of the Hopf bifurcation one has $\omega_c=\mathrm{Im}(\sigma)$, and Eq. (44) can be decomposed into its real and imaginary parts. From these two equations $f_{cat}^{(0)}$ and ω_c are determined by standard methods. c_{0c} may be calculated via Eq. (22).

1. Traveling waves solutions

At the Hopf bifurcation, the nonstationary part of growing microtubules is again described by the distribution given by Eq. (37b) and the fields c_{oli} and c_d are not in phase with c_t, in general. The two fields may be written in terms of the amplitude ratio $|E|$ and the relative phase φ_d in the following form:

$$c_t^{(1)}=2A\cos(\omega_c t), \tag{45a}$$

$$c_d^{(1)}=2A|E|\cos(\omega_c t+\varphi_d). \tag{45b}$$

The amplitude ratio $|E|$ and the phase φ_d can be determined from the two coupled equations (41b), and (41c), and they are given by

$$|E|=\frac{\sqrt{f_{cat}^{(0)2}+\omega_c^2[G(f_{cat}^{(0)2}+\omega_c^2)-1]^2}}{\alpha G(f_{cat}^{(0)2}+\omega_c^2)},$$

$$\varphi_d=\arctan\left(\frac{\omega_c}{f_{cat}^{(0)}}[G(f_{cat}^{(0)2}+\omega_c^2)-1]\right). \tag{46}$$

In a similar manner the oligomer density $c_{oli}^{(1)}$ may be written in terms of an amplitude ratio $|F|$ and a relative phase φ_{oli} between $c_{oli}^{(1)}$ and $c_t^{(1)}$,

$$c_{oli}^{(1)} = 2A|F|\cos(\omega_c t + \varphi_{oli}), \tag{47}$$

with

$$|F| = \frac{\sqrt{\alpha^2+\omega_c^2}}{\chi}|E|,$$

and

$$\varphi_{oli} = \arctan\left(\frac{\alpha\tan(\varphi_d)+\omega_c}{\alpha-\omega_c\tan(\varphi_d)}\right). \tag{48}$$

The oscillatory contribution to the polymerized tubulin $L^{(1)}$ can also be written as a harmonic function, $L^{(1)} = 2A|H|\cos(\omega_c t+\varphi_L)$. For both, the amplitude ratio $|H|$ and the relative phase φ_L, one obtains long expressions that are not presented here. The phase shifts and the amplitude ratios between the oscillating fields are shown in Fig. 7 as functions of the regeneration rate α. As discussed in Sec. IV A, the phase shift of the polymerized tubulin $L^{(1)}(t)$ with respect to $c_t^{(1)}$ is rather independent of α, whereas the phase of oligomer oscillations changes slightly with α. A phase shift π between the polymerized tubulin and oligomers is measured in experiments, cf. Refs. [12,34]. In this model this is only possible in the limit of a dissociation rate χ much smaller than the regeneration rate α.

2. Numerical results for the threshold of model II

At the threshold, one has again $\sigma = i\omega_c$, and from the imaginary part together with the real part of the dispersion relation in Eq. (44), the critical concentration c_{0c} and the Hopf frequency ω_c may be calculated as functions of the parameters. Also for model II we restrict our numerical calculations to the catastrophe rate with the exponential dependence given in Eq. (3).

The critical tubulin concentration c_{0c} and the critical frequency ω_c at the Hopf bifurcation are shown in Fig. 6 as functions of the regeneration rate α and for two different values of the decay rate of oligomers χ, whereby for the reduced parameter G the value $G=3000$ has been chosen. Since G includes a number of parameters, the curves in both parts represent a larger parameter set. For a fixed finite value for χ in the limit of a vanishing regeneration $\alpha\to 0$, where the polymerization cycle is interrupted, and in the limit of very large values of α, where the regeneration process is much faster than any other process, the critical tubulin concentration c_{0c} diverges similar to model I and, therefore, the Hopf bifurcation is suppressed. If α is kept fixed at a medium value, the threshold curve $c_{0c}(\chi)$ as a function of the decay rate χ for oligomers has a similar shape, as shown as a function of α in Fig. 6. The critical tubulin concentration c_{0c} also takes its smallest values at intermediate values of α, χ and G, whereby the location of the threshold minima depends on the actual values of the rest of parameters. With a decreasing rate $\alpha\to 0$ of tubulin regeneration, also the frequency ω_c becomes small. On the other hand, for large values of α, the tubulin regeneration is not anymore a rate limiting factor and the critical frequency ω_c becomes rather independent of α, cf. Sec. IV A 1.

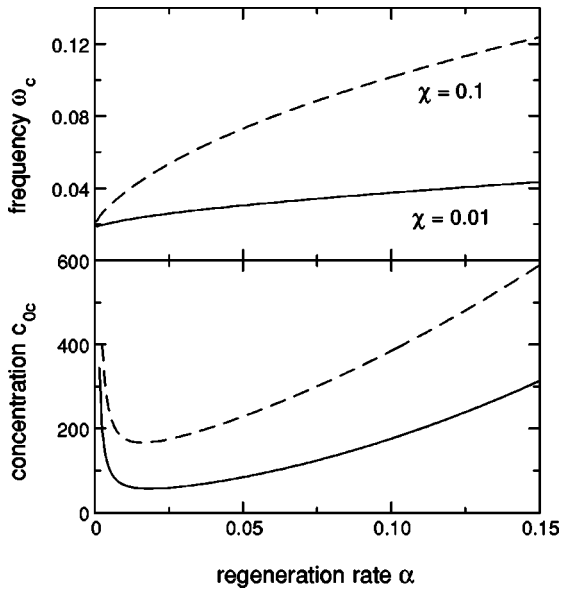

FIG. 6. For model II the critical tubulin concentration c_{0c} and the critical frequency ω_c are shown at the Hopf bifurcation as functions of the regeneration rate α and for two different values of the decay rate χ of oligomers. The rest of the parameters are $G=3000$, $f=0.1$, and $c_f=3$.

The stability of oligomers and, therefore, the decay rate χ depend very much on the available GTP: Increasing GTP concentrations destabilize oligomers and increase the decay rate χ [7,11]. With increasing GTP concentrations, also the rate α of the transition from c_d to c_t is enhanced. However, if the tubulin regeneration and the oligomer decay become too quick, an oscillatory polymerization is suppressed. In other words, if one increases α and χ beyond some minimum values, the threshold concentration for tubulin increases too. Such a tendency for the GTP dependence of the oscillation is in agreement with the results reported from experiments [7,11,12].

With increasing values of α, tubulin-d is again quickly transferred by the regeneration process into tubulin-t, leading to a small amplitude ratio $c_d^{(1)}/c_t^{(1)}$. Accordingly more tubulin is left to be stored in $L^{(1)}$ and $c_{oli}^{(1)}$. Therefore, both increase with larger values of α as indicated in Fig. 7. This has to be compared with $L^{(1)}$ for model I, where it decays as a function of α, because the phase shift between the contributions of the growing and shrinking microtubules changes too. For model II, the relative phases are also rather independent of α, whereby due to the quick regeneration of c_d the relative phase between $c_t^{(1)}$ and $c_d^{(1)}$ is slightly decreasing.

3. Reduced models

The dispersion relation for models I and II, considered in the preceding section, becomes equivalent in the limits $\beta\to 0$ and $\chi\to\infty$, and in both cases one obtains the same dispersion relation

$$\sigma^3 G f_{cat}^{(0)} + \sigma^2[G\alpha f_{cat}^{(0)} + 2G f_{cat}^{(0)2}] + \sigma[\alpha(1+2G f_{cat}^{(0)^2}) + G f_{cat}^{(0)^3} + f_{cat}^{(0)}] + \alpha f_{cat}^{(0)}[2+G f_{cat}^{(0)^2}] + f_{cat}^{(0)^2} = 0, \tag{49}$$

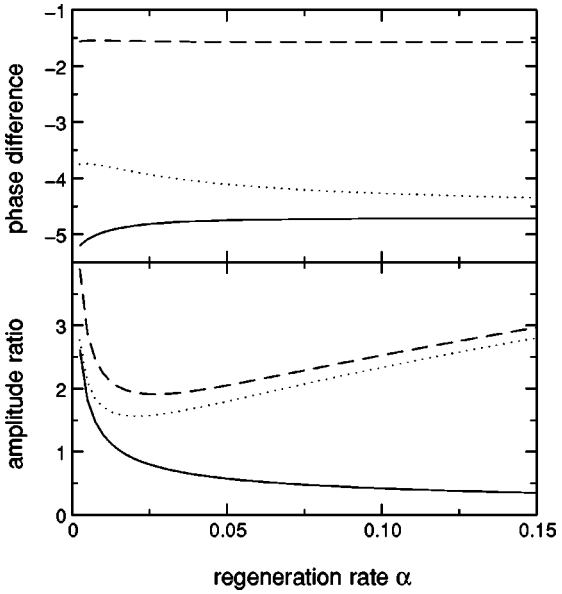

FIG. 7. The phase differences (upper part) and the amplitude ratios (lower part) between the oscillating contributions to the tubulin-*d* concentration $c_d^{(1)}$ (solid), the oligomer concentration $c_{oli}^{(1)}$ (dotted), and the total polymerized tubulin $L^{(1)}(t)$ (dashed) with respect to the tubulin-*t* concentration $c_t^{(1)}$ are shown as a function of the regeneration rate α. The other parameters are $G=3000$ and $\chi=0.02$.

with the reduced parameter G as given in Eq. (30) for model I and with $G=c_f/(\eta\lambda v_g \nu)$ for model II. This polynomial in σ always has negative growth rates, $\mathrm{Re}(\sigma)<0$, and, therefore, stationary solutions are always stable.

V. NUMERICAL METHOD FOR MODEL I

The two differential equations for growing and shrinking microtubules in Eqs. (6) are of first order with respect to the length l of the microtubules and first order in time. A straightforward spatial discretization of such first-order equations often leads to numerical instabilities. Especially, the equation for shrinking microtubules, cf. Eq. (6b), has problematic stability properties. For this reason, we approximate the solutions of Eqs. (6) by a two-mode ansatz

$$p_g(l,t)=\exp\left(-\frac{f_{cat}^{(0)}}{v_g}l\right)\left(\frac{\nu}{v_g}+F_g(l,t)\right), \tag{50a}$$

$$p_s(l,t)=\exp\left(-\frac{f_{cat}^{(0)}}{v_g}l\right)\left(\frac{\nu}{v_s}+F_s(l,t)\right), \tag{50b}$$

where the first mode describes just the stationary solution and the second one describes the oscillatory contribution. This approximation becomes exact close to the threshold and this ansatz leads with Eqs. (6) to two differential equations for $F_{g,s}$,

$$\partial_t F_g=(f_{cat}^{(0)}-f_{cat})\left(\frac{\nu}{v_g}+F_g\right)-v_g\partial_l F_g, \tag{51a}$$

$$\partial_t F_s=f_{cat}\left(\frac{\nu}{v_g}+F_g\right)-\frac{v_s}{v_g}f_{cat}^{(0)}\left(\frac{\nu}{v_s}+F_s\right)+v_s\partial_l F_s. \tag{51b}$$

Both fields may be expanded with respect to the first two spatial Fourier modes e^{inlk} $(n=0,1)$,

$$F_g(l,t)=B(t)+\tfrac{1}{2}[C(t)e^{ikl}+C^*(t)e^{-ikl}], \tag{52a}$$

$$F_s(l,t)=D(t)+\tfrac{1}{2}[H(t)e^{ikl}+H^*(t)e^{-ikl}], \tag{52b}$$

in order to remove the spatial dependence from Eqs. (51). Herein, the wave number is chosen at its value at the threshold of the Hopf bifurcation, $k=\omega_c/v_g$. This ansatz leads to a set of ordinary differential equations for the time-dependent amplitudes $B(t),C(t),D(t),H(t)$ that are described in the following.

Due to Eq. (5) one has the boundary condition $F_g(l=0,t)=0$ that gives the relation $C_R=-B$, with $\mathrm{Re}(C)=C_R$, between these two functions. Ansatz (52a) together with Eq. (51a) leads to the relation

$$\mathrm{Im}(C)=C_I=\frac{\nu}{kv_g^2}(f_{cat}-f_{cat}^{(0)}), \tag{53}$$

and to the first-order differential equation in B,

$$\partial_t B=(f_{cat}^{(0)}-f_{cat})\left(\frac{\nu}{v_g}+B\right). \tag{54}$$

Ansatz (52b) in Eq. (51b) gives the set of coupled differential equations

$$\partial_t D=f_{cat}\left(\frac{\nu}{v_g}+B\right)-\frac{\nu f_{cat}^{(0)}}{v_g}-\frac{v_s}{v_g}f_{cat}^{(0)}D, \tag{55a}$$

$$\partial_t H_R=-f_{cat}B-\frac{v_s}{v_g}f_{cat}^{(0)}H_R-kv_sH_I, \tag{55b}$$

$$\partial_t H_I=f_{cat}C_I-\frac{v_s}{v_g}f_{cat}^{(0)}H_I+kv_sH_R. \tag{55c}$$

With the periodic l dependence given in Eqs. (52), the integrals in Eq. (24c) can be evaluated, and one obtains the following differential equation for the tubulin-*t* dimer density:

$$\partial_t c_t=-\gamma v_g K(t)-\alpha\gamma L(t)+\alpha c_{0c}(1+\varepsilon)-\alpha c_t, \tag{56}$$

where the coefficients are given by

$$K(t)=\int_0^\infty dl\, p_g(l,t)=\frac{\nu}{v_g\delta}+\frac{k(kB-\delta C_I)}{\delta(\delta^2+k^2)}, \tag{57}$$

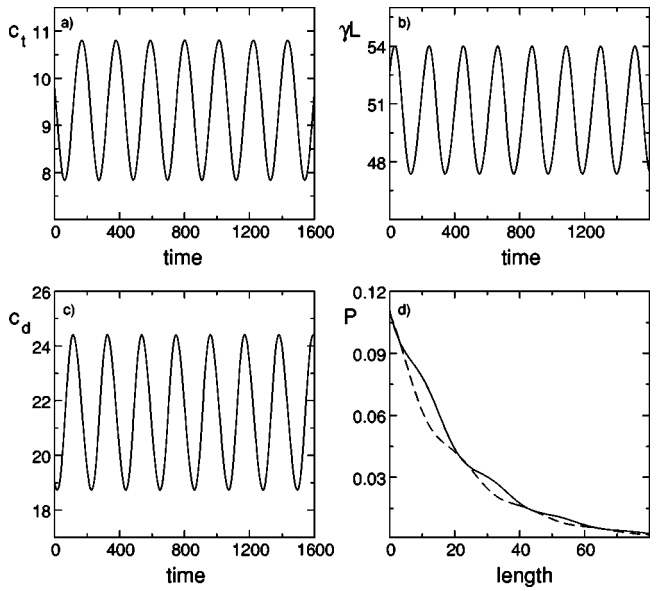

FIG. 8. For model I, the time dependence of the tubulin-*t* concentration $c_t(t)$, the polymerized tubulin $\gamma L(t)$, and the tubulin-*d* concentration $c_d(t)$ is shown in parts (a), (b), and (c), respectively. The parameters $\nu=0.01$, $\alpha=0.01$, $\beta=0.1$ were used with the corresponding critical initial concentration $c_{0c}=80.69$. The reduced control parameter is chosen at the value $\varepsilon=0.01$. In part (d) the length distribution of the microtubules $P(l)=p_g(l)+p_s(l)$ is shown at two different times $t=876$ (solid) and $t=975$ (dashed), where $\gamma L(t)$ takes its maximum and minimum, respectively.

$$L(t)=\int_0^\infty dl\, l[p_g(l,t)+p_s(l,t)]$$

$$=\frac{\nu}{\delta^2}\left(\frac{1}{v_g}+\frac{1}{v_s}\right)+\Delta[3\delta^2k^2B+k^4B-2\delta^3kC_I$$

$$+\delta^2(\delta^2-k^2)H_R-2\delta^3kH_I+(\delta^2+k^2)^2D], \quad (58)$$

and where the variables $\Delta=[\delta^2(\delta^2+k^2)^2]^{-1}$ and $\delta=f_{cat}^{(0)}/v_g$ have been introduced. The reduced control parameter $\varepsilon=(c_0-c_{0c})/c_{0c}$ measures the difference between the tubulin dimer concentration c_0 and the critical one c_{0c}. For $\varepsilon>0$, sustained oscillations occur but they are damped below threshold, $\varepsilon<0$. For the numerical solution of model II we use either the same approximation scheme, where only the factors of the scheme take a different form, or in the absence of p_s a direct spatial discretization provides also a stable algorithm. The five differential equations for model I in Eqs. (54), (55), and (56) and the corresponding three differential equations for model II are integrated numerically by a second-order Runge-Kutta method with a time step $\Delta t=0.01$.

The time dependence of the fields of model I are shown in Fig. 8 for one parameter set and these fields obviously have different phases. The extrema (maxima) of the polymerized tubulin $L(t)$ and the tubulin-*d* concentration $c_d(t)$ are delayed with respect to the extrema of the tubulin-*t* concentration $c_t(t)$, a behavior that is already indicated by the reaction cycle shown in Fig. 1. At the threshold, the parameter dependence of these phase differences may be calculated from the formulas given in Secs. IV A 3 and IV B 1. In Figs. 5 and 7, these phases are shown as functions of the regeneration rate α. In Fig. 8 the initial concentration of tubulin c_0 was chosen very close to the threshold c_{0c} with $\varepsilon=0.01$. At this value of the control parameter, the oscillations behave harmonically and the agreement between the numerical solution and the amplitude approximation is rather good, as described in the following section. For larger values of the reduced control parameter, the oscillations become anharmonic.

As already been mentioned in the Introduction, the length distribution of filaments is a crucial difference between the biochemical reaction discussed in this work and the common oscillatory chemical reactions. For model I, we show in Fig. 8(d) at two different times and at $\varepsilon=0.01$ the superposition of the length distribution of growing and shrinking microtubules, cf. $P(l)=p_g(l)+p_s(l)$. The exponential decay of the envelope of the length distribution is described by Eqs. (37b) and (37c), with a decay rate $v_g/f_{cat}^{(0)}$, and the modulation is due to the traveling waves in the time-dependent contribution. The amplitude of the shrinking microtubules is rather small for $\beta=0.1$ [cf. Eq. (37c)] and, therefore, the contribution to $P(l)$ comes mainly from growing microtubules.

For model II, a discretization of the length coordinate in the equation for growing microtubules, cf. Eq. (2), also provides a stable numerical algorithm. Hence, the nonlinear oscillatory solution can be obtained numerically without the approximations as described for model I in Eqs. (50) above. The respective results are shown in Figs. 9(a)–9(c), where the densities L, c_t, and c_{oli} are shown as functions of time for three different regeneration rates α. For both values of α in parts (a) and (b), the tubulin concentration is smaller than the corresponding threshold value, but the absolute distance c_0-c_{0c} to the threshold is equal. These transient subthreshold oscillations are remarkable, because the transient oscillations in experiments might be subthreshold ones, in contrast to the common interpretation that the oscillations are transient due to the tubulin-*t* consumption during the microtubule polymerization.

For the simulations shown in Fig. 9, a narrow length distribution p_g has been used as initial condition. In such cases, the tubulin-*t* concentration corresponds almost to the total initial concentration c_0. Starting with such an initial condition, at first tubulin-*t* dimers are consumed during the growth of microtubules. This leads to a first maximum of the polymerized tubulin L, but the oligomers, the decay product of the microtubules, are negligible and as a consequence the densities of tubulin-*d* and tubulin-*t* drop down too. But a small c_t increases the catastrophe rate f_{cat} and microtubules decay with a higher rate, which increases the density of oligomers, etc. After a few such oscillations, the densities reach their stationary values for subthreshold concentrations. In the case of a large regeneration rate the oscillation frequency is much higher than for small regeneration rates and more oscillations are performed until the stationary values are reached. The stationary value of the polymerized tubulin and of the oligomers is also much larger in part (b) than in part

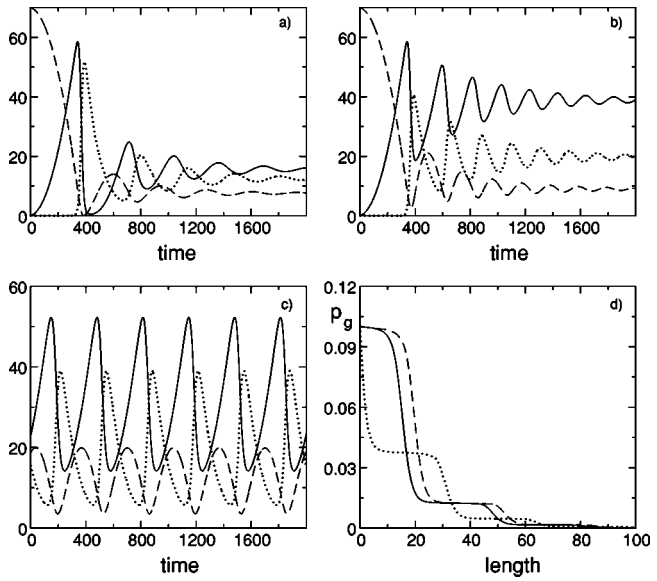

FIG. 9. For model II the time dependences of the polymerized tubulin $\eta\lambda L$ (solid), c_t (dashed), and c_{oli} (dotted) are shown below the Hopf bifurcation (see Fig. 6) for $\alpha=0.0036$ in (a) and for $\alpha=0.08$ in (b) with an initial concentration $c_0=70$. The corresponding critical concentration for both values of α is $c_{0c}=134.15$. The stationary value of the tubulin-d concentration is $c_d^{(0)}=2.465$ in (a) and $c_d^{(0)}=34.305$ in (b). In (c) the time dependence is shown beyond the oscillation threshold at $\alpha=0.01$. In part (d) the length distribution of the growing microtubules $p_g(l)$ is plotted at three different times. Both in (c) and (d) the initial concentration is $c_0=80$ and the critical tubulin concentration is $c_{0c}=65.97$, which corresponds to the value $\varepsilon=0.21$ for the reduced control parameter. The maximal length of the growing microtubules has been chosen as $12v_g/f_{cat}^{(0)}$. In all parts, the rest of the parameters are $\nu=0.01$, $\chi=0.01$, $v_g=0.1$.

(a), whereas the stationary value for the tubulin-t dimers remains nearly constant. The reason is the low density c_d in the case of large values of α.

Far beyond the threshold of the Hopf bifurcation, the oscillations become anharmonic as shown in Fig. 9(c). Hereby the oscillations of the total polymerization and of their decay product, c_{oli}, are nearly in antiphase, similar as in experiments described in Ref. [7]. At the threshold, a phase difference of π was only possible in the limit of large regeneration rates α and for a much smaller dissociation rate χ. If we consider initial concentrations that are much larger than the corresponding critical concentration, the phase shift of π between $L(t)$ and $c_{oli}(t)$ is also possible at intermediate values of χ and α.

In Fig. 9(d) the distribution for growing microtubules $p_g(l)$ is shown for model II at three different times. The reduced control parameter $\varepsilon=0.21$ is rather large compared to its value in Fig. 8, and the curves indicate that the length distribution of microtubules is not described anymore by harmonic traveling waves as in the vicinity of the bifurcation. As long as the tubulin-t density is large and the catastrophe rate small, microtubules grow with a constant velocity v_g and only a few of them experience a catastrophe. During this period, a plateau in the length distribution is built. But after a large amount of tubulin-t has been used up, the catastrophe rate f_{cat} increases very steeply, leading to a strong decay of the microtubules at all lengths. If f_{cat} drops down again, the low density of long microtubules grows further with a constant velocity v_g and short microtubules are nucleated at a higher density. This leads to a step in the distribution that travels with the growth velocity v_g to larger values of l. Therefore, far beyond the oscillatory threshold, the temporally anharmonic behavior of c_t leads in this manner to the steplike length distribution of the microtubules.

VI. AMPLITUDE EXPANSION

Here we focus on a semianalytical treatment of the oscillating polymerization slightly beyond its onset. The interesting question here is whether the bifurcation to these oscillations is continuous (supercritical) or discontinuous (subcritical). In physical systems, Hopf bifurcations are mostly subcritical [27,35], but for the models discussed in this work we always find a supercritical one. This is advantageous, because for a supercritical Hopf bifurcation a semianalytical treatment is possible. The appropriate framework is the universal amplitude equation of oscillatory fields, cf. Eq. (1). This equation will be derived in the present section from the basic reaction equations of microtubule polymerization.

The perturbation analysis employed for the derivation of Eq. (1) is an expansion of the solutions of the basic equations with respect to small amplitudes of the oscillatory contributions [27,28]. As a small perturbation parameter, the relative difference between the actual tubulin concentration c_0 and the critical tubulin concentration c_{0c} is introduced,

$$\varepsilon=\frac{c_0-c_{0c}}{c_{0c}}. \tag{59}$$

A signature for the $\pm$ symmetry of the oscillatory behavior [27,28] is the power law for the oscillation amplitude $A\sim\sqrt{\varepsilon}$. Accordingly, the solutions of the basic equations at the threshold are expanded with respect to powers of $\sqrt{\varepsilon}$,

$$\mathbf{u}=\mathbf{u}^{(0)}+\varepsilon^{1/2}\mathbf{u}^{(1)}+\varepsilon\mathbf{u}^{(2)}+\varepsilon^{3/2}\mathbf{u}^{(3)}+O(\varepsilon^2), \tag{60}$$

where the vector notation $\mathbf{u}^{(j)}=(\tilde{p}_g^{(j)},\tilde{p}_s^{(j)},\tilde{c}_t^{(j)})$ is used with $j=0,1,2,3$. The components of $\mathbf{u}^{(j)}$ differ by a factor of $\sqrt{\varepsilon}$, such as $\sqrt{\varepsilon}\tilde{c}_t^{(1)}=c_t^{(1)}$, etc. The components of $\mathbf{u}^{(0)}$ describe the stationary microtubule polymerization as given in Sec. III and the components of $\mathbf{u}^{(1)}$ describe the linear oscillatory solutions that may be written at the threshold in the following form:

$$\mathbf{u}^{(1)}=B\mathbf{u}_e e^{i\omega_c t}+\text{c.c.} \tag{61}$$

Here $\mathbf{u}_e$ includes the amplitude ratios between the fields $c_t^{(1)}$, $p_g^{(1)}$, $p_s^{(1)}$ at the threshold and $\sqrt{\varepsilon}B=A$ as explained below.

Close to the threshold, one has $\mathrm{Re}(\sigma)\sim\varepsilon\ll 1$, and the linear solution $\mathbf{u}^{(1)}\sim e^{\sigma t}$ grows or decays only by a very small amount during one oscillation period $2\pi/\omega_c$. These two disparate time scales near the threshold, that of the os-

cillation period ($\propto 2\pi/\omega_c$) and that of growth and decay ($\propto 1/\varepsilon$), may be separated within a perturbation expansion by introducing a slow time scale $T=\varepsilon t$ [27,28]. The fast time scale is included in the exponential function $e^{i\omega_c t}$, and the other one will be described by a slowly varying amplitude $B(T)$. Accordingly, the linear solution near threshold may be written as

$$\mathbf{u}^{(1)}(t,T)=B(T)\mathbf{u}_e e^{i\omega_c t}+\text{c.c.} \tag{62}$$

In order to differentiate this product of time-dependent functions, instead of applying the chain rule of differentiation, one may replace this operation by the following sum: $\partial_t \rightarrow \partial_t+\varepsilon\partial_T$. Here ∂_t acts only on the fast time dependence occurring in the exponential function and ∂_T acts only on the amplitude $B(T)$.

Using this replacement and the ε expansion of $\mathbf{u}$ the basic equations given in Sec. II can be ordered with respect to powers of $\sqrt{\varepsilon}$. In this way we obtain a hierarchy of partial differential equations, which we need up to $O(\varepsilon^{3/2})$. The whole procedure is described in greater detail in the Appendix. The amplitude equation follows from a solubility condition for the equation at order $O(\varepsilon^{3/2})$ and it has the following form:

$$\tau_0\partial_T B=(1+ia)B-g(1+ic)|B|^2B. \tag{63}$$

τ_0 is the relaxation time, a and c are the linear and nonlinear frequency shifts, respectively. The nonlinear coefficient g determines the bifurcation structure. For $g>0$ the bifurcation is supercritical (steady) and for $g<0$ the bifurcation is subcritical (unsteady). For the coefficients τ_0, a, g, and c, one obtains long expressions in terms of the reaction constants of the basic equations, which have been calculated by using computer algebra. The respective formulas are not presented, but the parameter dependence of the coefficients is shown in Fig. 10 for model I and in Fig. 11 for model II.

Rescaling the time $T=\varepsilon t$ and amplitude $A=\sqrt{\varepsilon}B$ back to the original units yields the amplitude equation

$$\tau_0\partial_t A=\varepsilon(1+ia)A-g(1+ic)|A|^2A, \tag{64}$$

as introduced in Sec. I. This equation has simple nonlinear oscillatory solutions of the form $A=Fe^{i\Omega t}$, with an amplitude F and a frequency Ω as follows:

$$F=\sqrt{\frac{\varepsilon}{g}},$$

$$\Omega=\frac{1}{\tau_0}(\varepsilon a-gcF^2)=\frac{a-c}{\tau_0}\varepsilon. \tag{65}$$

Ω describes the deviation of the oscillation frequency from the critical one, ω_c.

The linear coefficients τ_0 and a of Eq. (64) may directly be calculated from the dispersion relation in Eq. (29) or Eq. (44) in the following way. The solution $A=0$ of Eq. (64) corresponds to the stationary polymerization described in Sec. III, which is stable in the range $\varepsilon<0$ against small perturbations $A\sim\tilde{F}e^{\sigma t}$ (with $\tilde{F}\ll\sqrt{|\varepsilon|}$) and unstable for $\varepsilon>0$. Neglecting in Eq. (64) the contributions due to the cubic nonlinearity, one obtains from its linear part the dispersion relation $\sigma=\varepsilon(1+i(a)/\tau_0$. This formula gives the relaxation time τ_0 and the linear frequency dispersion a in terms of derivatives of the growth rate with respect to the control parameter ε: $\tau_0=[\partial\,\mathrm{Re}(\sigma)/\partial\varepsilon]^{-1}$ and $a=\tau_0\partial\,\mathrm{Re}(\sigma)/\partial\varepsilon$. If ε is expressed in terms of the dimer density c_0, cf. Eq. (59), then both quantities may also be written in terms of the derivatives with respect to c_0,

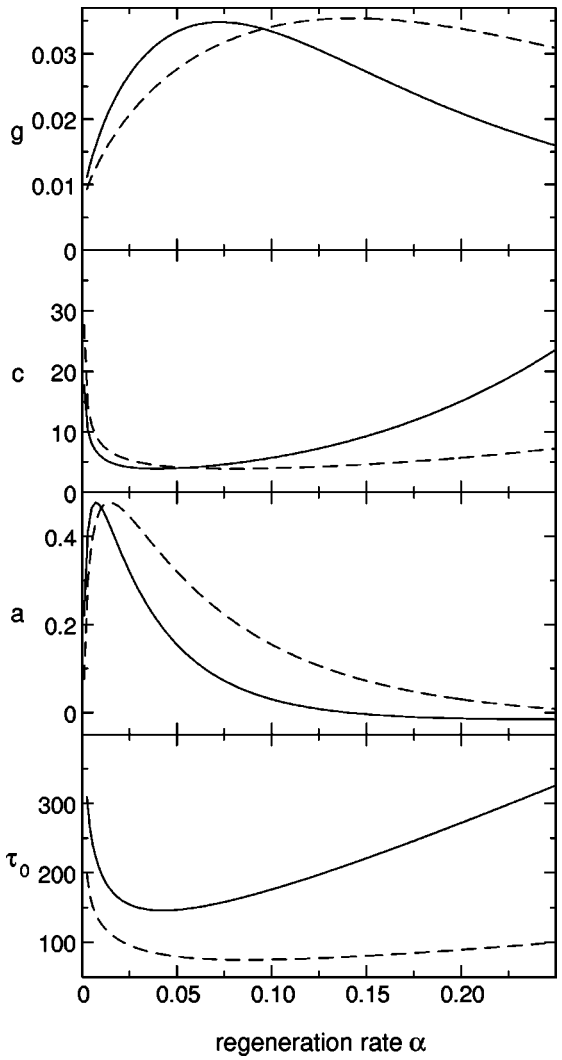

FIG. 10. The coefficients τ_0, a, g, and c of the amplitude equation (64) are shown for model I as functions of the regeneration rate α and for two different nucleation rates $\nu=0.01$ (solid line) and $\nu=0.04$ (dashed). For the rest of the parameters, the values $v_g=0.1$, $\beta=0.1$, $f=0.1$, and $c_f=3$ have been chosen.

$$\tau_0=\frac{1}{c_{0c}\partial\,\mathrm{Re}(\sigma)/\partial c_0},\quad a=c_{0c}\tau_0\frac{\partial\,\mathrm{Im}(\sigma)}{\partial c_0}, \tag{66}$$

whereby both derivatives are taken at the threshold concentration c_{0c}. The dispersion relations $\sigma(\varepsilon)$, as obtained on the one hand by the amplitude equation and on the other hand by solving Eq. (29) or Eq. (44), both have to reproduce the growth or decay dynamics of small perturbations with

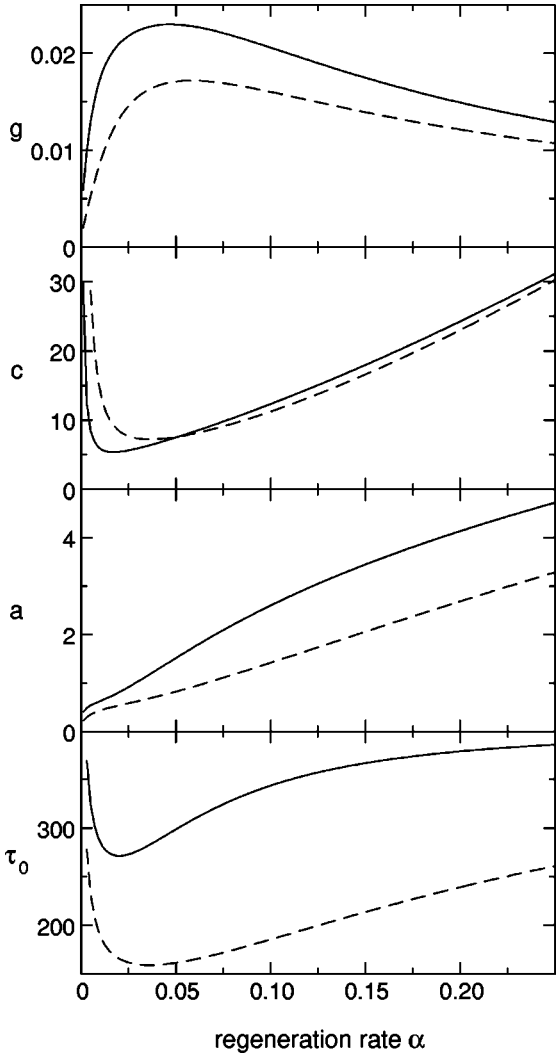

FIG. 11. The linear and nonlinear coefficients of the amplitude equation (64) are shown for model II as functions of the regeneration rate α and for two different nucleation rates $\nu=0.01$ (solid) and $\nu=0.04$ (dashed). For the rest of the parameters the values $\chi=0.01$, $f=0.1$, $c_f=3$ have been chosen.

respect to the stationary polymerization. Therefore, the coefficients τ_0 and a of the amplitude equation can directly be calculated via Eq. (66) from the numerical solutions of Eq. (29) or Eq. (44).

One aim of the amplitude expansion is the determination of the type of the Hopf bifurcation. For two different nucleation rates $\nu=0.01$ and $\nu=0.04$, the variation of the nonlinear coefficient g as a function of the regeneration rate α is shown for model I in Fig. 10 (top) and for model II with oligomer dynamics in Fig. 11. In both cases, g behaves rather similar and is positive for the models investigated in this work. Therefore the Hopf bifurcation is supercritical. In Figs. 10 and 11, the nonlinear coefficient g increases at first with the regeneration rate α and reaches a maximum in a range where the threshold concentration $c_{0c}(\alpha)$ takes its minimum.

It should be mentioned that, for a given value of the control parameter ε, a large value of g corresponds to a small value of the oscillation amplitude. Since the threshold

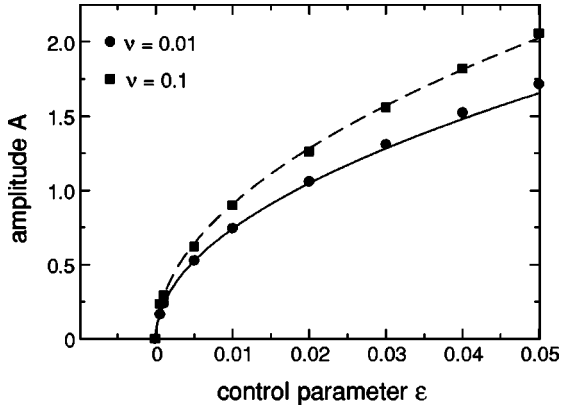

FIG. 12. The amplitude of the oscillations as a function of the reduced control parameter ε and for two different nucleation rates ν. The solid line is the result of the amplitude equation and data points have been determined from simulations as described in Sec. V. The parameters that have been used are $\gamma=1$, $\alpha=0.01$, $v_g=0.1$, $\beta=0.1$, $f=0.1$, $c_f=3$.

$c_{0c}(\alpha)$ varies too, the variation of the oscillation amplitude with α is much less when $c_{0c}\varepsilon$ is kept constant. According to the sign of the nonlinear coefficient c, the oscillation frequency $\omega_c+\Omega$ decreases with increasing values of ε. The results in terms of the amplitude equation are in fairly good agreement with the behavior of the full numerical solution of the basic reaction equations.

A determination of the bifurcation structure by numerical simulations of the basic equations is error prone compared to the results of perturbation calculation described here. Besides the lower accuracy, parameter studies such as in Figs. 10 and 11 are much more time consuming with numerical simulations.

Close to threshold, the advantages of the perturbation calculation are obvious. However, it is *a priori* unknown to which ε range the amplitude equation approach (64) applies quantitatively. For some systems the amplitude equation is valid in a rather large range of the control parameter ε, but for other systems its validity is restricted to very small values of it, cf. Ref. [27]. In order to check this for our models of microtubule polymerization, we compare in Fig. 12 the variation of the oscillation amplitude of $c_t^{(1)}$ with the control parameter ε as obtained by the numerical solution described in Sec. V and by the solution $A=\sqrt{\varepsilon/g}$ of the amplitude equation for two different values of the nucleation rate ν. At larger values of the control parameter, $\varepsilon=0.1$, the difference between the results for the numerical solution and the amplitude equation is still less than 8%. For model II the deviations are larger between the amplitude determined by the amplitude equation approach and the numerical solutions with the ansatz in Eqs. (52). However, when we solve the equation for growing microtubules, cf. Eq. (2), numerically by discretization of the length coordinate, the deviations become smaller.

For both models, the linear coefficient τ_0 and the nonlinear coefficients g,c do not differ very much from each other. However, the linear frequency shift a increases in model II for large regeneration rates α, whereas for model I it de-

creases. Nevertheless, in both models the nonlinear frequency correction due to the values of c is much larger than the linear correction due to a, $c \gg a$.

Whether the bifurcation to oscillatory polymerization is also supercritical in experiments under stationary regeneration conditions is an open question. Therefore an experimental determination of the bifurcation type would be an important test for the reduced models investigated in this work.

The variation of the other coefficients with the regeneration rate α provides further contact between the model parameters and experimentally measurable quantities. The parameters c, a, and τ_0 may be determined as follows. Studying the growth of small perturbations, $c_t^{(1)} \propto e^{\mathrm{Re}(\sigma)t} = e^{\varepsilon t/\tau_0}$, by plotting the logarithm $\varepsilon t/\tau_0 \propto \ln(c_t^{(1)})$ as a function of time and for different values of ε, the relaxation time τ_0 may be determined. In a similar manner, a may be determined by studying the frequency of a perturbation far below its nonlinear saturation amplitude. If the perturbation saturates finally, the oscillation frequency of the nonlinear solution changes with ε as indicated by Eq. (65). From this ε dependence the nonlinear coefficient c may be extracted. An experimental determination of these coefficients, as described, would be a further test of the basic model equations.

VII. SUMMARY AND CONCLUSION

Two reduced models that capture oscillating microtubule polymerization and the length distribution of the microtubule filaments, as described in Sec. II, have been analyzed. In both models, the complex biochemical reaction steps of microtubule polymerization are described by a few steps, which have been identified in experiments to be important. The focus on a few essential degrees of freedom leads to some simplicity of the models that allows, for instance, a derivation of analytical expressions for the threshold and the oscillation frequency at the Hopf bifurcation. Such analytical results make trends as functions of the reaction rates more easily visible. Some of these trends may be tested in experiments and some of the reaction constants may be measured.

At threshold, also analytical expressions could be derived for the temporal evolution of the concentrations and the length distribution of microtubules. These provide a detailed picture of the temporal variation of the fields, their relative phases, and the amplitude ratios between them. The formula for the length distribution is especially instructive, cf. Eq. (37b); it describes a superposition of amplitude oscillations of the distribution and traveling waves, where the waves always travel towards larger lengths. This qualitative behavior of the length distribution during oscillatory polymerization is rather independent of the respective model and is a rather general feature. A few snapshots of the numerically generated distribution far beyond threshold are shown in Fig. 9(b). The distribution includes still traveling waves, but far beyond threshold, these behave rather anharmonic.

For stationary reaction conditions, as assumed in this work, Fig. 9 shows a remarkable result. In parts (a) and (b) of this figure, a subthreshold concentration for tubulin was assumed, i.e., $c_0 < c_{0c}$, and in both cases the final state is stationary polymerization. However, on the route to the stationary state, transient oscillations occur. Therefore, the transient character of the microtubule oscillations observed in an experiment with an enzymatic regeneration process for GTP [11], could have, according to the results described in this work, its origin in a too low tubulin concentration. A higher tubulin concentration or an appropriate regeneration rate of GTP and a different lifetime of oligomers could lead, in a similar experiment, to persistent microtubule oscillations.

For transient oscillations observed in other experiments, the common interpretation is as follows. During the microtubule polymerization in experiments, the available GTP is used up and the oscillations last only for a few periods. If GTP is continuously supplied, the simultaneously increasing amount of GTD inhibits various reactions steps and slows down the reaction cycle. The results shown in Figs. 9(a) and 9(b) indicate that oscillations may occur as a transient because either GTP is used up or the tubulin concentration has only a subthreshold value. Accordingly, there may be several reasons for transient oscillations in experiments. Either the initial tubulin concentration has a subthreshold value, the decay rate of oligomers and the regeneration rate for GTP do not have their optimal values, which would explain transient oscillations in experiments with a regenerative enzyme system, or the reaction conditions are not constant, because GTP is used up. In the latter case the available tubulin-t decreases with time and the microtubule polymerization decays.

In an *in vitro* experiment with constant reaction conditions, the threshold of oscillations might be measured by increasing the tubulin dimer concentration by appropriate steps. Immediately after each step, transient oscillations might occur, but the threshold is only crossed when the oscillations persist over a long time.

In order to avoid numerical instabilities during long time simulations of the reaction equations, including Eq. (6b), we use analytical approximations for the length dependence of the microtubule distributions as described in Sec. V. This stable numerical scheme can be generalized in future work to an effective algorithm for dealing with microtubule polymerization in one and two spatial dimensions [26], in order to investigate spatial patterns occurring during polymerization of microtubules [10,24]. The respective extension of the amplitude equation may also lead to interesting insights.

Microtubule filaments at a high density show an isotropic-nematic phase transition [22], similar to what has been observed for F-actin filaments [36]. Since the early theory of Onsager [37], this transition for rods in a solvent is a well understood phenomenon [38]. For a monodisperse distribution of filaments of fixed length, i.e., without polymerization kinetics, many aspects of the isotropic-nematic transition have been understood. For polydisperse rod mixtures, some aspects of the isotropic-nematic transition can be considered to be understood too [39]. The effects of nucleation, growth of filaments, and the decay of filaments on the isotropic-nematic transition are not known at present and one may expect interesting phenomena related to this kinetics [23]. The effect of oscillating microtubule polymerization on the isotropic-nematic transition is also completely unexplored at present and will be investigated in forthcoming works [23].

ACKNOWLEDGMENTS

It is a great pleasure to thank M. Breidenich, H. Flyvbjerg, E. Mandelkow, H. Müller-Krumbhaar, J. Prost, and J. Tabony for interesting discussions.

APPENDIX: AMPLITUDE EXPANSION FOR MODEL I

For model I and the catastrophe rate given in Eq. (3), the major steps of the derivation of the amplitude equation (1) are described in this appendix. Since we neglect the rescue of shrinking microtubules, $f_{resc}=0$, the only nonlinear term in the basic equations of model I is the product $f_{cat}(c_t)p_g$ in Eq. (6). At first we expand the concentrations c_t, c_0 and length distributions $p_{g,s}$ with respect to deviations from their stationary value at the threshold for oscillation, such as, for instance, for the tubulin-t concentration, i.e., $c_t - c_t^{(0)} = \sqrt{\varepsilon}\tilde{c}_t^{(1)} + \varepsilon\tilde{c}_t^{(2)} + \cdots$. Note that the fields having tildes differ just by a power of $\sqrt{\varepsilon}$ from the fields without tildes as introduced in Sec. IV, cf. $(\sqrt{\varepsilon})^j \tilde{c}_t^{(j)} = c_t^{(j)}$, etc. In order to simplify the notation of this appendix we drop the tilde and the expansion of the catastrophe rate takes the form

$$f_{cat} = f_{cat}^{(0)} + \varepsilon^{1/2} f_{cat}^{(1)} + \varepsilon f_{cat}^{(2)} + \varepsilon^{3/2} f_{cat}^{(3)} + \cdots, \tag{A1}$$

whereby the coefficients of this expansion are

$$f_{cat}^{(1)} = -f_{cat}^{(0)} \frac{c_t^{(1)}}{c_f}, \tag{A2a}$$

$$f_{cat}^{(2)} = f_{cat}^{(0)} \left[\frac{1}{2} \left(\frac{c_t^{(1)}}{c_f} \right)^2 - \frac{c_t^{(2)}}{c_f} \right], \tag{A2b}$$

$$f_{cat}^{(3)} = f_{cat}^{(0)} \left[\frac{c_t^{(1)} c_t^{(2)}}{c_f^2} - \frac{c_t^{(3)}}{c_f} - \frac{1}{6} \left(\frac{c_t^{(1)}}{c_f} \right)^3 \right]. \tag{A2c}$$

Collecting in Eqs. (6) and (11) the contributions to the order $\varepsilon^{1/2}$, we recover the linear equations given in Sec. IV:

$$\partial_t p_g^{(1)} = f_{cat}^{(0)} \frac{c_t^{(1)}}{c_f} p_g^{(0)} - f_{cat}^{(0)} p_g^{(1)} - v_g \partial_l p_g^{(1)}, \tag{A3a}$$

$$\partial_t p_s^{(1)} = -f_{cat}^{(0)} \frac{c_t^{(1)}}{c_f} p_g^{(0)} + f_{cat}^{(0)} p_g^{(1)} + v_s \partial_l p_s^{(1)}, \tag{A3b}$$

$$\partial_t c_t^{(1)} = -\gamma \int_0^\infty dl [v_g p_g^{(1)} + \alpha l (p_g^{(1)} + p_s^{(1)})] - \alpha c_t^{(1)}. \tag{A3c}$$

At order ε, we obtain the three equations

$$\partial_t p_g^{(2)} = \left(f_{cat}^{(0)} \frac{c_t^{(2)}}{c_f} p_g^{(0)} - f_{cat}^{(0)} p_g^{(2)} - v_g \partial_l p_g^{(2)} \right) + f_{cat}^{(0)} \frac{c_t^{(1)}}{c_f} p_g^{(1)} - \frac{f_{cat}^{(0)}}{2} \left(\frac{c_t^{(1)}}{c_f} \right)^2 p_g^{(0)}, \tag{A4a}$$

$$\partial_t p_s^{(2)} = \left(-f_{cat}^{(0)} \frac{c_t^{(2)}}{c_f} p_g^{(0)} + f_{cat}^{(0)} p_g^{(2)} + v_s \partial_l p_s^{(2)} \right) - f_{cat}^{(0)} \frac{c_t^{(1)}}{c_f} p_g^{(1)} + \frac{f_{cat}^{(0)}}{2} \left(\frac{c_t^{(1)}}{c_f} \right)^2 p_g^{(0)}, \tag{A4b}$$

$$\partial_t c_t^{(2)} = -\gamma \int_0^\infty dl [v_g p_g^{(2)} + \alpha l (p_g^{(2)} + p_s^{(2)})] + \alpha c_{0c} - \alpha c_t^{(2)}. \tag{A4c}$$

With the solutions of the equations at the previous order $\varepsilon^{1/2}$, which are already given in Sec. IV A 3, the equations at order ε have to be solved. These solutions have the following form:

$$c_t^{(2)} = A_0 + A_2 \exp(2i\omega_c(t) + \text{c.c.}, \tag{A5a}$$

$$p_g^{(2)} = e^{-f_{cat}^{(0)} l / v_g} \{ B_0(l) + [B_2(l) e^{2i\omega_c t} + \text{c.c.}] \}, \tag{A5b}$$

$$p_s^{(2)} = e^{-f_{cat}^{(0)} l / v_g} \{ D_0(l) + [D_2(l) e^{2i\omega_c t} + \text{c.c.}] \}, \tag{A5c}$$

whereby the expressions for the coefficients A_0, A_2, B_i, and D_i are rather lengthy in terms of the coefficients of the solutions at order $\varepsilon^{1/2}$ and are not given here.

The equations at the next higher order $\varepsilon^{3/2}$ are

$$\begin{aligned} \partial_T p_g^{(1)} + \partial_t p_g^{(3)} = {} & \left(f_{cat}^{(0)} \frac{c_t^{(3)}}{c_f} p_g^{(0)} - f_{cat}^{(0)} p_g^{(3)} - v_g \partial_l p_g^{(3)} \right) \\ & - \left[f_{cat}^{(0)} \frac{c_t^{(1)} c_t^{(2)}}{c_f^2} - \frac{f_{cat}^{(0)}}{6} \left(\frac{c_t^{(1)}}{c_f} \right)^3 \right] p_g^{(0)} \\ & + \left[f_{cat}^{(0)} \frac{c_t^{(2)}}{c_f} - \frac{f_{cat}^{(0)}}{2} \left(\frac{c_t^{(1)}}{c_f} \right)^2 \right] p_g^{(1)} \\ & + f_{cat}^{(0)} \frac{c_t^{(1)}}{c_f} p_g^{(2)}, \end{aligned} \tag{A6a}$$

$$\begin{aligned} \partial_T p_s^{(1)} + \partial_t p_s^{(3)} = {} & \left(-f_{cat}^{(0)} \frac{c_t^{(3)}}{c_f} p_g^{(0)} + f_{cat}^{(0)} p_g^{(3)} + v_s \partial_l p_s^{(3)} \right) \\ & + \left[f_{cat}^{(0)} \frac{c_t^{(1)} c_t^{(2)}}{c_f^2} - \frac{f_{cat}^{(0)}}{6} \left(\frac{c_t^{(1)}}{c_f} \right)^3 \right] p_g^{(0)} \\ & - \left[f_{cat}^{(0)} \frac{c_t^{(2)}}{c_f} - \frac{f_{cat}^{(0)}}{2} \left(\frac{c_t^{(1)}}{c_f} \right)^2 \right] p_g^{(1)} \\ & - f_{cat}^{(0)} \frac{c_t^{(1)}}{c_f} p_g^{(2)}, \end{aligned} \tag{A6b}$$

$$\partial_T c_t^{(1)} + \partial_t c_t^{(3)} = -\gamma \int_0^\infty dl [v_g p_g^{(3)} + \alpha l (p_g^{(3)} + p_s^{(3)})] - \alpha c_t^{(3)}. \tag{A6c}$$

The two fields $p_g^{(3)}$ and $p_s^{(3)}$ have to be calculated explicitly at this order from Eqs. (A6a) and (A6b) as well. With both solutions, the integral on the right hand side of Eq. (A6c) can

be calculated. Equation (A6a) and (A6b) include both contributions proportional to $e^{i\omega_c t}$ and $e^{3i\omega_c t}$, but only the single-harmonic terms are relevant in Eq. (A6c). The coefficient of $e^{i\omega_c t}$ in Eq. (A6c) must vanish. Part of it vanishes automatically, because it reproduces the threshold condition, and the rest provides the amplitude equation with all the coefficients now given in terms of the reaction rates of the basic equations.

[1] B. Alberts *et al*., *Molecular Biology of the Cell* (Garland, New York, 1994); H. Lodish *et al.*, *Molecular Cell Biology* (Freeman, New York, 1999); J. Howard, *Mechanics of Motor Proteins and the Cytoskeleton* (Sinauer, Sunderland, 2001).

[2] A. Desai and T.J. Mitchison, Annu. Rev. Cell Dev. Biol. **13**, 83 (1997); A. Hyman and E. Karsenti, J. Cell. Sci. **111**, 2077 (1998).

[3] O. Valiron, N. Caudron, and D. Job, Cell. Mol. Life Sci. **58**, 2069 (2001).

[4] T.J. Mitchison and M. Kirschner, Nature (London) **312**, 232 (1984); **312**, 237 (1984).

[5] F. Pirolet, D. Job, R. Margolis, and J. Garel, EMBO J. **6**, 3247 (1987).

[6] M.F. Carlier *et al.*, Proc. Natl. Acad. Sci. U.S.A. **84**, 5257 (1987).

[7] E.-M. Mandelkow, G. Lange, A. Jagla, U. Spann, and E. Mandelkow, EMBO J. **7**, 357 (1988).

[8] G. Lange, E.-M. Mandelkow, A. Jagla, and E. Mandelkow, Eur. J. Biochem. **178**, 61 (1988).

[9] R. Melki, M.F. Carlier, and D. Pantaloni, EMBO J. **7**, 2653 (1988).

[10] E. Mandelkow *et al.*, Science **246**, 1291 (1989).

[11] R. Wade, F. Pirollet, R. Margolis, J. Garel, and D. Job, Biol. Cell **65**, 37 (1989).

[12] E.M. Mandelkow and E. Mandelkow, Cell Motil. Cytoskeleton **22**, 235 (1992).

[13] Y. Chen and T.L. Hill, Proc. Natl. Acad. Sci. U.S.A. **84**, 8419 (1987).

[14] M. Dogterom and S. Leibler, Phys. Rev. Lett. **70**, 1347 (1993).

[15] A. Marx and E. Mandelkow, Eur. Biophys. J. **22**, 405 (1994).

[16] B. Houchmandzadeh and M. Vallade, Phys. Rev. E **53**, 6320 (1996).

[17] E. Jobs, D.E. Wolf, and H. Flyvbjerg, Phys. Rev. Lett. **79**, 519 (1997).

[18] D. Sept, H.J. Limbach, H. Bolterauer, and J.A. Tuszynski, J. Theor. Biol. **197**, 77 (1999).

[19] J. Tabony and D. Job, Proc. Natl. Acad. Sci. U.S.A. **89**, 6948 (1992).

[20] P. Gray and S.K. Scott, *Chemical Oscillations and Instabilities* (Clarendon, Oxford, 1994).

[21] J.J. Tyson, *The Belousov-Zhabotinskii Reaction* (Springer, Berlin, 1976).

[22] A.L. Hitt, A.R. Cross, and J.R.C. Williams, J. Biol. Chem. **265**, 1639 (1990).

[23] F. Ziebert and W. Zimmermann (unpublished).

[24] J. Tabony and D. Job, Nature (London) **346**, 448 (1990); J. Tabony, Science **264**, 245 (1994); J. Tabony, Proc. Natl. Acad. Sci. U.S.A. **97**, 8364 (2000).

[25] F.J. Nedelec, T. Surrey, A.C. Maggs, and S. Leibler, Nature (London) **389**, 305 (1997); T. Surrey, F. Nedelec, S. Leibler, and E. Karsenti, Science **292**, 116 (2001).

[26] M. Hammele and W. Zimmermann (unpublished).

[27] M.C. Cross and P.C. Hohenberg, Rev. Mod. Phys. **65**, 851 (1993); A.C. Newell, T. Passot, and J. Lega, Annu. Rev. Fluid Mech. **25**, 399 (1992).

[28] S.H. Strogatz, *Nonlinear Dynamics and Chaos* (Addison-Wesley, New York, 1994).

[29] I. Aranson and L. Kramer, Rev. Mod. Phys. **74**, 99 (2002).

[30] N. Caudron *et al.*, J. Mol. Biol. **297**, 211 (2000).

[31] D.K. Fygenson, E. Braun, and A. Libchaber, Phys. Rev. E **50**, 1579 (1994).

[32] H. Flyvbjerg, E. Jobs, and S. Leibler, Proc. Natl. Acad. Sci. U.S.A. **93**, 5975 (1996).

[33] A. Marx *et al.*, in *Synchrotron Radiation in the Biosciences* (Clarendon, Oxford, 1994), p. 158.

[34] H. Oberman, E.M. Mandelkow, G. Lange, and E. Mandelkow, J. Biol. Chem. **265**, 4382 (1990).

[35] W. Schöpf and W. Zimmermann, Phys. Rev. E **47**, 1739 (1993).

[36] A. Suzuki, T. Maeda, and T. Ito, Biophys. J. **59**, 25 (1991); C.M. Coppin and P.C. Leavis, *ibid.* **63**, 794 (1992); R. Furukawa, R. Kundra, and M. Fechheimer, Biochemistry **32**, 12 346 (1993); J. Käs *et al.*, Biophys. J. **70**, 609 (1996).

[37] L. Onsager, Ann. N. Y. Acad. Sci. USA **51**, 627 (1949).

[38] P.G. de Gennes and J. Prost, *The Physics of Liquid Crystals* (Clarendon, Oxford, 1993).

[39] G.J. Vroege and H.N.W. Lekkerkerker, Rep. Prog. Phys. **1241**, 55 (1992).